Density Perturbations in Hybrid Inflation Using a Free Field Theory Time-Delay Approach

Alan H. Guth and Evangelos I. Sfakianakis*

Center for Theoretical Physics, Laboratory for Nuclear Science and Department of Physics,

Massachusetts Institute of Technology, Cambridge, MA 02139, USA

(Dated: September 25, 2018)

We introduce a new method for calculating density perturbations in hybrid inflation which avoids treating the fluctuations of the "waterfall" field as if they were small perturbations about a classical trajectory. We quantize only the waterfall field, treating it as a free quantum field with a time-dependent m^2, which evolves from positive values to tachyonic values. Although this potential has no minimum, we think it captures the important dynamics that occurs as m^2 goes through zero, at which time a large spike in the density perturbations is generated. We assume that the time-delay formalism provides an accurate approximation to the density perturbations, and proceed to calculate the power spectrum of the time delay fluctuations. While the evolution of the field is linear, the time delay is a nonlinear function to which all modes contribute. Using the Gaussian probability distribution of the mode amplitudes, we express the time-delay power spectrum as an integral which can be carried out numerically. We use this method to calculate numerically the spectrum of density perturbations created in hybrid inflation models for a wide range of parameters. A characteristic of the spectrum is the appearance of a spike at small length scales, which can be used to relate the model parameters to observational data. It is conceivable that this spike could seed the formation of black holes that can evolve to become the supermassive black holes found at the centers of galaxies.

---

*Electronic address: guth@ctp.mit.edu; esfaki@mit.edu

I.   INTRODUCTION

Inflation [1] remains the leading paradigm for the very early universe. It naturally solves the cosmological flatness and horizon problems and is consistent with high precision measurements of the cosmic microwave background radiation [2, 3]. Numerous models of inflation have been proposed, each adding features to the predictions of a scale invariant spectrum derived from single-field slow-roll inflation. Their motivation can be either some particle physics ideas coming from the standard model [4] or supersymmetric theories [5, 6], the need to explain some observation such as glitches in the CMB or supermassive black holes in galactic centers, or simply the extension of a theorist's toolbox in anticipation of the next set of high precision data, such as the upcoming Planck satellite measurements.

Hybrid inflation was first proposed by A. Linde [7] and the name was chosen because this class of models can be thought of as being a hybrid between chaotic inflation and inflation in a theory with spontaneous symmetry breaking. The simplest hybrid inflation model requires two fields that we will call the timer and waterfall fields. The timer field corresponds the usual slow rolling field and is responsible for the scale invariant spectrum of perturbations observed in the CMB. The waterfall field is confined to its origin by the interaction with the timer field, giving a large constant contribution to the potential, which is also the main contribution to the energy density and hence the Hubble parameter. The potential governing the waterfall field changes as the timer field evolves, and at some point the minimum of the potential turns into a local maximum, and the waterfall field rolls down its tachyonic potential to its new minimum, where inflation ends. A characteristic feature of the density perturbation spectrum of hybrid inflation is the appearance of a large spike generated at the time when the waterfall potential turns tachyonic. The spike is generically at small length scales, and can potentially seed primordial black holes [8]. Primordial black hole formation and evolution has been studied in the past [9–12], but whether these black holes grow to become the supermassive black holes currently found in galactic centers is an open and intriguing possibility that we will address in a future publication.

Usual inflationary perturbation theory is based on the study of quantum fluctuations around a classical trajectory in field space. However, in a purely classical formulation the waterfall field of hybrid inflation would remain forever at the origin, even after the waterfall transition, due to symmetry. It is quantum fluctuations that destabilize it and lead to the

end of inflation, so in a sense the classical trajectory has a quantum origin. Numerous papers have used various analytical approaches or numerical simulations to overcome this difficulty and approximate the spectrum of density perturbations [5, 6, 13–21].

The method we use here has evolved from the early work in Kristin Burgess' thesis [13], in which she studied a free-field model of the waterfall field in one space dimension, focusing on the time delay of the scalar field as a measure of perturbations. As in the model considered here, the waterfall field was described by a Lagrangian with a time-dependent m^2, caused by the interaction with the timer field. m^2 evolved from positive values at early times to negative (tachyonic) values at late times. Such models are unnatural, since the potential is not bounded from below, but they nonetheless appear to be useful toy models, since the dynamics that generate the spike in the fluctuation spectrum occur during the transition from positive to negative m^2. The evolution in the bottomless potential is realistic enough to give a well-defined time delay. Burgess studied the evolution of the waterfall field by means of a numerical simulation on a spatial lattice, using 262,000 points, calculating the power spectrum of the time delay by Monte Carlo methods. The method was slow, but for one choice of parameters she accumulated 5000 runs, giving a very reliable graph of the time-delay spectrum for this model. This line of research was pursued further in the thesis of Nguyen Thanh Son [14], who repeated Burgess' numerical simulations with a new code (with excellent agreement). More importantly, Son and one of us (AHG), with some crucial input from private communication with Larry Guth, developed a method to short-circuit the Monte Carlo calculation. Instead of determining the power spectrum by repeated random trials, it was possible to express the expectation value for the random trials as an explicit expression involving integrals over mode functions, which could be evaluated numerically. The speed and numerical precision were dramatically improved. While Son's work was still limited to one spatial dimension, the possibility of extending it to three spatial dimensions was now a very realistic goal. In this paper we extend the calculation of the time-delay power spectrum in free-field models of hybrid inflation to three spatial dimensions, calculating the spectrum for a wide range of model parameters.

In Section II we define the free-field model for the timer and waterfall fields that we will use to calculate fluctuations. We set up the equations of motion, define the notation of the mode expansion, and discuss the behavior of the mode functions. We make contact with a class of supersymmetric models that support hybrid inflation in Section III, presenting

the form of their potential and the range of parameters that they allow. Section IV gives a brief summary of the time delay formalism, and presents an approximation for calculating perturbations, developed earlier by Randall, Soljačić, and Guth. In Section V we develop a new method for calculating density perturbations in hybrid inflation that avoids any need to consider small fluctuations about a classical solution. Instead we show how the time delay power spectrum can be calculated essentially exactly in the context of the free field theory description. The result is given in the form of an integral over the modes which makes use of their known Gaussian probability distribution. In section VI we present an extensive set of numerical results over the parameter space of our model, where we are able to isolate the main factors that influence the density perturbation spectrum. In the limit of a light timer field, all quantities of interest are determined by the product of the timer and waterfall masses. We examine the models discussed in Section II as examples of realistic versions of hybrid inflation, and provide graphs showing the predictions of these models. Concluding remarks and directions of future work follow in Section VII.

II.   MODEL

A.   Field set-up

Our first assumption is related to the expansion rate. We consider the metric to be exactly De-Sitter, even though this is only approximately correct. However, it changes only weakly during the slow roll inflation era, and we will terminate our calculation once the approximation loses its validity. Defining the Hubble constant during inflation as H, the scale factor is written as

$$a(t) = e^{Ht} \tag{1}$$

The model consists of two scalar fields. The "waterfall" field ϕ with lagrangian

$$L_\phi = e^{3Ht} \left[|\dot{\phi}|^2 - e^{-2Ht} |\nabla \phi|^2 - m_\phi^2(t) |\phi|^2 \right] \tag{2}$$

The usual 1/2 factors can be restored, if one writes $\phi = \frac{1}{\sqrt{2}} (\phi_1 + i\phi_2)$ where ϕ_1 and ϕ_2 are real scalar fields. The waterfall field must be complex, otherwise it will create domain walls as it rolls down from its initial value. The time-dependent mass of the ϕ field is controlled by a real scalar field, subsequently called the "timing" field. The important property of the

squared mass of ϕ is that it has to be positive initially and as ψ evolves become negative. A general form is the following

$$m_\phi^2(t) = -m_0^2 \left[1 - \left(\frac{\psi(t)}{\psi_c}\right)^r\right] \tag{3}$$

We will choose $r = 4$ for most of our simulations. The lagrangian of the timing field is

$$L_\psi = e^{3Ht} \left[\frac{1}{2}\dot{\psi}^2 - \frac{1}{2}e^{-2Ht}(\nabla\psi)^2 - \frac{1}{2}m_\psi^2\psi^2\right] \tag{4}$$

The Lagrangians define the system up to an additive constant V_0 in the potential, which is taken to be large enough, so that the variations in H are negligible during the era of interest. We neglected the interaction term from the Lagrangian of the timing field. This means that there is no back-reaction from the waterfall to the timing field. Physically this is a reasonable approximation before the waterfall transition, as well as afterwards, for as long as the waterfall field remains close to the origin. Mathematically, neglecting this term makes the equation of motion for the timing field de-coupled and in our quadratic approximation analytically solvable.

Furthermore we do not examine perturbations arising from quantum fluctuations of the timing field. Before the waterfall transition they will give the nearly scale invariant spectrum that can be matched to the CMB observations. Apart from making sure that the long wavelength tail of the waterfall field perturbations does not contradict WMAP data, we will not consider these scales. After the waterfall transition the timer field perturbations will continue to be of the order of 10^{-5}, hence they will be subdominant to the perturbations of the waterfall field by a few orders of magnitude, as we will see. The equations of motion are

$$\ddot{\phi} + 3H\dot{\phi} - e^{-2Ht}\nabla^2\phi = -m_\phi^2(t)\phi \tag{5}$$

$$\ddot{\psi} + 3H\dot{\psi} - e^{-2Ht}\nabla^2\psi = -m_\psi^2\psi \tag{6}$$

If we take the timing field to be spatially homogenous, we get

$$\psi(t) = \psi_c e^{pt} \ , \ p = H\left(-\frac{3}{2} \pm \sqrt{\frac{9}{4} - \frac{m_\psi^2}{H^2}}\right) \tag{7}$$

The value of the constant of integration was chosen so that $\psi(t) = \psi_c$ and $m_\phi^2(t) = 0$ at $t = 0$. Both roots are negative, but the long time behavior is dominated by the larger of the two roots, which is

$$p = -H\left(\frac{3}{2} - \sqrt{\frac{9}{4} - \frac{m_\psi^2}{H^2}}\right) \tag{8}$$

We will always choose $\frac{m_\psi}{H} < 3/2$ and not consider the case of a complex root. In fact, hybrid inflation models usually require the mass of the timing field to be well below the Hubble parameter, as in [5] and [6]. We choose to measure time in number of e-folds, hence we use $N = Ht$. We rescale the masses similarly as $\mu_\psi = m_\psi/H$ and $\mu_\phi = m_0/H$. Furthermore the finite box size that we will use in our simulations is measured in units of $\frac{1}{H}$ and the field magnitude in units of H. We also define

$$\tilde{\mu}_\psi^2 = -\frac{rp}{H} = r\left(\frac{3}{2} - \sqrt{\frac{9}{4} - \frac{m_\psi^2}{H^2}}\right) \tag{9}$$

For a light timer field the reduced mass $\tilde{\mu}_\psi$ is proportional to the actual timer mass, $\tilde{\mu}_\psi = \sqrt{\frac{r}{3}}\left(\frac{m_\psi}{H}\right) = \sqrt{\frac{r}{3}}\mu_\psi$.

B. Fast Transition

Let's consider the speed of the transition. The transition happens at $m_\phi^2 = 0$. In order to quantify the speed of the transition, we will use the basic scale of our system, the Hubble scale. We will consider the transition duration to be the period for which $|m_\phi| \le H$, meaning that the mass term in the equation of motion of the waterfall field is negligible. Assuming that $\tilde{\mu}_\phi > 1$ we get

$$\pm 1 = \mu_\phi^2\left(1 - e^{-\tilde{\mu}_\psi^2 N}\right) \Rightarrow \Delta N = \frac{1}{\tilde{\mu}_\psi^2}\log\left(\frac{\mu_\phi^2 + 1}{\mu_\phi^2 - 1}\right) \tag{10}$$

In the limit of $\tilde{\mu}_\phi \gg 1$

$$\Delta N = \frac{2}{(\tilde{\mu}_\psi \mu_\phi)^2} \tag{11}$$

Another measure of the speed of the transition is given by derivative of the waterfall field mass at $N = 0$.

$$\frac{1}{H^2}\frac{dm_\phi^2(N)}{dN}\Big|_{N=0} = (\tilde{\mu}_\psi \mu_\phi)^2 \Rightarrow \Delta N \sim \frac{1}{(\tilde{\mu}_\psi \mu_\phi)^2} \tag{12}$$

This shows that as long as the product $\mu_\phi \mu_\psi$ is somewhat larger than unity, the duration of the transition will be less than a Hubble time, meaning that the transition is fast!

C. Mode expansion

For purposes of our numerical calculations, we think of the universe as a finite box with periodic boundary conditions and a discrete spatial lattice. We choose the lattice to be cubic

with length b and Q^3 points. This means that

$$\vec{x} = \frac{b}{Q}\vec{l} \ , \quad \vec{k} = \frac{2\pi}{b}\vec{n} \ , \tag{13}$$

where $\vec{l}$ is a triplet of integers between 0 and $Q-1$ and $\vec{n}$ is a triplet of integers between $-Q/2$ and $(Q/2)-1$. We can move between the finite discrete set of points and the continuous limit using the usual substitutions

$$\int d^3x \to \left(\frac{b}{Q}\right)^3 \sum_{\vec{x}} \ , \quad \int d^3k \to \left(\frac{2\pi}{b}\right)^3 \sum_{\vec{k}} \ . \tag{14}$$

Our convention for the Fourier transform is

$$
\begin{aligned}
f(\vec{x}) &= \int d^3k \, e^{i\vec{k}\cdot\vec{x}} f(\vec{k}) = \left(\frac{2\pi}{b}\right)^3 \sum_{\vec{k}} e^{i\vec{k}\cdot\vec{x}} f(\vec{k}) \\
f(\vec{k}) &= \left(\frac{1}{2\pi}\right)^3 \int d^3x \, e^{i\vec{k}\cdot\vec{x}} f(\vec{x}) = \left(\frac{1}{2\pi}\right)^3 \left(\frac{b}{Q}\right)^3 \sum_{\vec{x}} e^{i\vec{k}\cdot\vec{x}} f(\vec{x}) \ .
\end{aligned}
\tag{15}
$$

We will expand the waterfall field in modes in momentum space,

$$\phi(\vec{x},t) = \frac{1}{(2\pi)^{3/2}} \left(\frac{2\pi}{b}\right)^{3/2} \sum_{\vec{k}} [c(\vec{k})e^{i\vec{k}\cdot\vec{x}} u(\vec{k},t) + d^\dagger(\vec{k})e^{-i\vec{k}\cdot\vec{x}} u^*(\vec{k},t)] \ , \tag{16}$$

which with Eq. (5) gives

$$\ddot{u}(\vec{k},N) + 3\dot{u}(\vec{k},N) + e^{-2N}\tilde{k}^2 u(\vec{k},N) = \mu_\phi^2(1 - e^{-\tilde{\mu}_\psi^2 N})u(\vec{k},N) \ , \tag{17}$$

where $\tilde{k} = \frac{|\vec{k}|}{H}$ and an overdot denotes a derivative with respect to the time variable $N = Ht$.

D. Solution of the mode function

1. Early time behavior

At asymptotically early times the $\tilde{k}^2$ term dominates over the mass term provided that $\tilde{\mu}_\psi^2 < 2$. For $r = 2$ this is the case for $\mu_\psi < \sqrt{2}$, and for $r = 4$ it holds for $\mu_\psi < \sqrt{5/4}$. These inequalities will hold throughout the parameter space of the models that we will examine, so we can neglect the mass term for $N \to -\infty$. We then define a new function, following [22] as

$$u(\vec{k},N) = \frac{1}{2}\sqrt{\frac{\pi}{H}} e^{-3N/2} Z(z) \ , \quad z = \tilde{k}e^{-N} \ . \tag{18}$$

Neglecting the mass term in Eq. (17), we find

$$z^2 \frac{d^2 Z}{dz^2} + z \frac{dZ}{dz} + \left(z^2 - \frac{9}{4} \right) Z = 0 \,, \tag{19}$$

which is the equation for a Bessel function of order $3/2$. At early times the solution should look like a harmonic oscillator in its ground state, or equivalently the ground state of a free field in flat space, which is composed of negative frequency complex exponentials. This choice of initial conditions is the well known Bunch–Davies vacuum. For a review of scalar field quantization in de Sitter space and the corresponding vacuum choice see for example Ref. [23]. At early times the solution is given by

$$u \sim \frac{1}{2} \sqrt{\frac{\pi}{H}} e^{-3N/2} H_{3/2}^{(1)}(z) \,, \tag{20}$$

where

$$H_{3/2}^{(1)}(z) = -\sqrt{\frac{2}{\pi z}} e^{iz} \left(1 - \frac{1}{iz} \right) \tag{21}$$

is a Hankle function, a linear combination of Bessel functions. (The phase is arbitrary, and the normalization is fixed by insisting that the field and the creation and annihilation operators obey their standard commutation relations.) Rewriting the original mode equation in terms of the new variable z, it simplifies to

$$\frac{\partial^2 u}{\partial z^2} - \frac{2}{z} \frac{\partial u}{\partial z} + u = \frac{\mu_\phi^2}{z^2} \left[1 - \left(\frac{z}{\tilde{k}} \right)^{\tilde{\mu}_\psi^2} \right] u \,. \tag{22}$$

The $\vec{k} = 0$ mode is not captured by the procedure described here and is presented in detail in Appendix A.

2. General Solution

We will now examine the general solution in a form that will be more appropriate for the numerical calculations that we have to perform. We can write the solution as

$$u(\vec{k}, t) = \frac{1}{\sqrt{2\tilde{k}H}} R(\vec{k}, t) e^{i\theta(\vec{k}, t)} \tag{23}$$

and the differential equation separates in real and imaginary parts

$$\ddot{R} - R\dot{\theta}^2 + 3\dot{R} + e^{-2N} \tilde{k}^2 R = \mu_\phi^2 (1 - e^{-\tilde{\mu}_\psi^2 N}) R \tag{24}$$

$$2\dot{R}\dot{\theta} + R\ddot{\theta} + 3R\dot{\theta} = 0 \tag{25}$$

Integrating the second equation gives

$$\dot{\theta} = const \frac{e^{-3N}}{R^2} \tag{26}$$

By comparing this with the early time behavior of the analytic solution

$$u \sim \frac{1}{2H\sqrt{\tilde{k}}} e^{-N} e^{i\tilde{k}e^{-N}} \tag{27}$$

the phase equation becomes

$$\dot{\theta} = -\frac{\tilde{k}e^{-3N}}{R^2} \tag{28}$$

while the initial condition for the amplitude is given by the same asymptotic term to be

$$R \to e^{-N} \tag{29}$$

Inserting this expression in the equation for the amplitude function R

$$\boxed{\ddot{R} - \frac{\tilde{k}^2 e^{-6N}}{R^3} + 3\dot{R} + e^{-2N}\tilde{k}^2 R = \mu_\phi^2 (1 - e^{-\tilde{\mu}_\psi^2 N})R} \tag{30}$$

3. A closer look at the mode behavior

Let us rewrite the equation of motion (Eq. 17) in a way that makes the time dependence of the solution more transparent

$$\ddot{u}_k(t) + 3\dot{u}_k(t) + \mu_{eff}^2 = 0 \quad , \quad \mu_{eff}^2(k) = \tilde{k}^2 e^{-2N} + \mu_\phi^2 e^{-\tilde{\mu}_\psi^2 N} - \mu_\phi^2 \tag{31}$$

We can distinguish different time windows with different behavior of the mode functions, based on the effective waterfall field mass. We will list these time windows here and then proceed to examine them one by one.

1. $N \ll 0$, many efolds before the waterfall transition, in the asymptotic past

2. $N_{dev}(k) < N < 0$, a few efolds before the transition, where $N_{dev}(k)$ is the time at which a mode starts deviating significantly from the e^{-N} behavior, in particular starts decaying faster.

3. $0 < N < N_{tr}(k)$ a few efolds after the transition, where $N_{tr}(k)$ is the time at which each mode starts growing.

4. $N \gg 0$, the asymptotic future

Now let us look at each of those time scales more closely. The asymptotic past is well described in the previous section and we see that all modes decay like e^{-N}. More precisely their magnitude behaves as $|u_k| \sim \sqrt{\frac{1}{2k}} e^{-N}$. The first time scale N_{dev} appears only for low wavenumbers. For $N < 0$ we can keep only two of the three terms in the effective mass. Since $\mu_\phi^2 e^{-\tilde{\mu}_\psi^2 N} > \mu_\phi^2$ we will drop the μ_ϕ^2 term, leaving the effective mass as $\mu_{eff}^2(k) = \tilde{k}^2 e^{-2N} + \mu_\phi^2 e^{-\tilde{\mu}_\psi^2 N}$. The time at which the two dominant terms become equal is

$$N_{dev}(k) = \frac{2}{2 - \tilde{\mu}_\psi^2} \log\left(\frac{\tilde{k}}{\mu_\phi}\right) \tag{32}$$

For $\tilde{k} \geq \mu_\phi$ this time is not negative, hence we cannot drop μ_ϕ^2 and our analysis fails. This transition, which happens only for $\tilde{k} < \mu_\phi$ signals a deviation of the behavior of the modes, which do not evolve as e^{-N}, but instead decay faster.

Next we move to the actual waterfall transition time for each mode, which happens when the effective squared mass changes sign and becomes negative, or

$$\tilde{k}^2 e^{-2N} = \mu_\phi^2 \left(1 - e^{-\tilde{\mu}_\psi^2 N}\right) \tag{33}$$

We will approximate the right hand side of the above equation with a piecewise linear function as follows

$$\mu_\phi^2 \left(1 - e^{-\tilde{\mu}_\psi^2 N}\right) = \begin{cases} \mu_\phi^2 \tilde{\mu}_\psi^2 N & : N < 1/\mu_\psi^2 \\ \mu_\phi^2 & : N > 1/\mu_\psi^2 \end{cases} \tag{34}$$

For $\tilde{k} < \mu_\phi e^{1/\mu_\psi^2}$ the solution is found on the first branch and is

$$N_{tr}(k) = \frac{1}{2} W\left(\frac{2\tilde{k}^2}{\mu_\phi \tilde{\mu}_\psi^2}\right) \tag{35}$$

where W is known as the Product Logarithm, or Lambert W function and is defined as the solution to the equation $z = W(z)e^{W(z)}$. For small values of the wavenumber we can write the solutions as a Taylor series in $\tilde{k}$

$$N_{tr}(\tilde{k} \ll \sqrt{\mu_\phi \tilde{\mu}_\psi}) = \frac{\tilde{k}^2}{\mu_\phi^2 \tilde{\mu}_\psi^2} + O(\tilde{k}^4) \tag{36}$$

For $\tilde{k} > \mu_\phi e^{1/\mu_\psi^2}$ we operate on the second branch and the transition time for each mode is

$$N_{tr}(k) = \log\left(\frac{\tilde{k}}{\mu_\phi}\right) \tag{37}$$

The behavior of the modes after the transition is different for different ranges of the timer field mass. If we consider the late time behavior of the mode equation, we can see two timescales introduced by the time dependent exponential coefficients. One is $O(1)$ and the other $O(1/\tilde{\mu}_\psi^2)$. We distinguish two cases: They can both be $O(1)$ or the second one can be larger than the first. The first timescale defines the time at which the equation becomes k-independent, meaning that all modes behave (grow) in the same way. The second time scale defines the time, after which the equation becomes time independent, meaning that after that all modes behave as pure exponentials.

Let us first deal with the case of $\tilde{\mu}_\psi \ll 1$ meaning that the second time scale is much larger than the first one. Between the two timescales, that is $1 < N < -1/\tilde{\mu}_\psi^2$, the equation is independent of $\tilde{k}$

$$\ddot{R} + 3\dot{R} = \mu_\phi^2(1 - e^{-\tilde{\mu}_\psi^2 N})R \tag{38}$$

Since the evolution of the exponential term on the right hand side is by far slowest than the other timescales in the problem, we will treat $1 - e^{-\tilde{\mu}_\psi^2 N}$ adiabatically. This leads immediately to the solution

$$R = R_0 e^{\lambda(N)N} \quad , \quad \lambda(N) = \frac{-3 + \sqrt{9 + 4\mu_\phi^2(1 - e^{-\tilde{\mu}_\psi^2 N})}}{2} \tag{39}$$

After a long time, this would mathematically settle to

$$\lambda_0 = \frac{-3 + \sqrt{9 + 4\mu_\phi^2}}{2} \ . \tag{40}$$

However, this is far beyond the time when inflation will have ended, hence it would physically never have time to happen (plus it is well outside the validity of our constructed potential).

Let us choose $\mu_\phi = 10$ and $\tilde{\mu}_\psi = 1/10$ to demonstrate our analysis. Some characteristic mode functions are presented in Fig. 1

We see that all modes behave similarly at late times, independent of their wave-number, as they should based on our late time analysis. Specifically, we can plot the ratio of the time derivative of each mode to its magnitude, as in Fig. 1. We call this the growth rate $\lambda \equiv \left(\frac{\dot{R}_k}{R_k}\right)$. We can see both phenomena. First, after $N \approx 6$ the modes behave identically. Second, the behavior of the mode approaches that of an exponential function (whose logarithm is a constant), but at a slower rate. In this example time needs to go on for several hundreds of efolds for the growth rate to set to a constant, which is calculated to be $\lambda(t \to \infty) = 8.6119$ for $\mu_\phi = 10$ and $\mu_\psi = 1/10$.
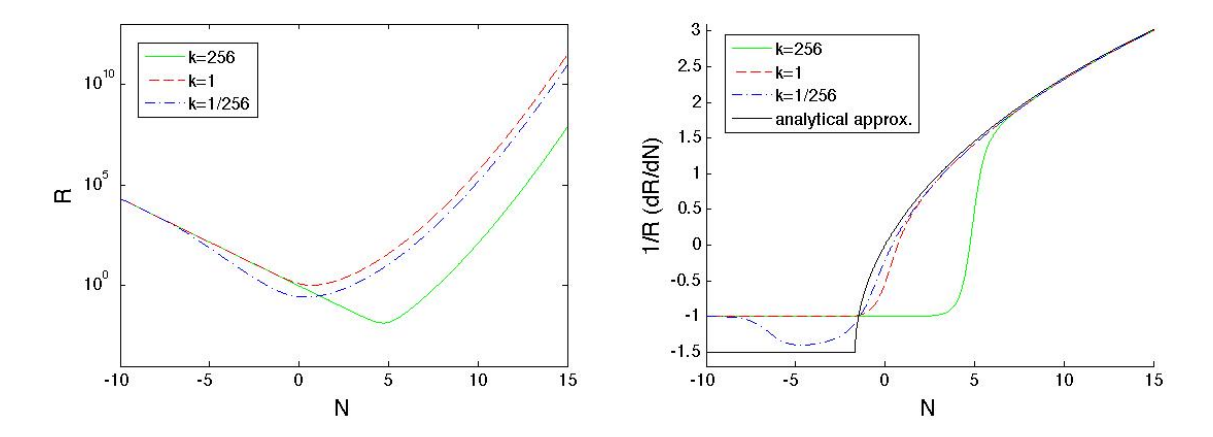
FIG. 1: Mode functions for different comoving wavenumbers as a function of time in efolds. The model parameters are $\mu_\psi = \frac{1}{10}$ and $\mu_\phi = 10$. We can see the modes following our analytic approximation for the growth rate. Our analysis gives $N_{dev}(1/256) \approx -7.9$ and $N_{tr}(256) \approx 4.76$, which are very close to the values that can be read off the graph.

It is important to test our analytical approach to the late time behavior of the growth rate of mode function. As seen in Fig. 1 once the mode functions evolve in a k - independent way, our simple analytical estimate for their growth rate is accurate to within a few percent, which gives us a very accurate expression for the growth rate and leads to the terms evolving as $u \sim e^{\lambda(t)t}$, where the time-dependent growth rate $\lambda(t)$ is slowly changing.

As a test of our analysis, we can calculate the two important transition times $N_{dev}(1/256) = -7.9005$ and $N_{tr}(256) = 4.76457$. We see that the calculated values agree very well with the behavior of the plotted modes.

Let us briefly examine the situation where $\tilde{\mu}_\psi^2 \leq 2$. In this case the mode equation becomes k-independent and time independent at about the same time, that is a few e-folds after the waterfall transition. We choose $\mu_\psi = \frac{1}{2}$ and $\mu_\phi = 1$ and plot the results in Fig. 2. It is clear that the modes become both k-independent and pure exponential (having a constant growth rate) at about the same time ($N \approx 10$). The asymptotic growth rate in this case is $\lambda(t \to \infty) = 0.3028$.

Again we can calculate the two important transition times $N_{dev}(1/256) = -7.8377$ and $N_{tr}(256) = 5.39554$, which agree once more with the behavior of the plotted modes.
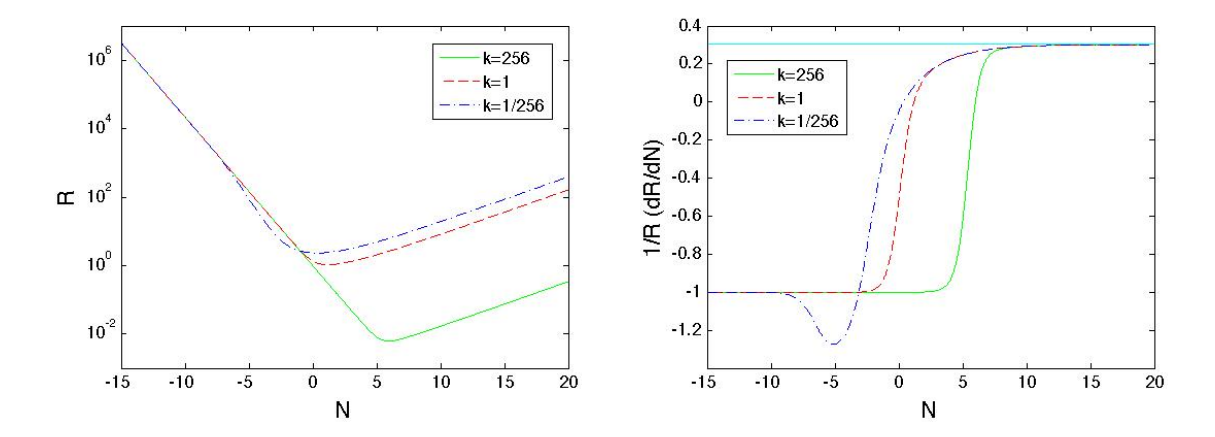
FIG. 2: Mode functions for different comoving wavenumbers as a function of time in efolds. The model parameters are $\mu_\psi = \frac{1}{2}$ and $\mu_\phi = 1$. The horizontal line corresponds to the asymptotic value of the growth factor λ. We can see how the mode functions reach their asymptotic behavior after 10 efolds. Our analysis gives $N_{dev}(1/256) \approx -7.84$ and $N_{tr}(256) \approx 5.4$, which are very close to the values that can be read off the graph.

III. SUPERNATURAL INFLATION MODELS

It is interesting to make contact between our abstract model and specific potentials inspired form particle theory. In general inflation models require small parameters in order to ensure slow roll inflation and produce the correct magnitude of density perturbations. It was shown in [5, 6] that supersymmetric theories with weak scale supersymmetry breaking can give models where such small parameters emerge "naturally" as ratios of masses already in the theory. We will not go into the details of such theories, but instead give the forms of the constructed potentials and use them as an application of our formalism.

$$V = M^4 \cos^2(\phi/\sqrt{2}f) + \frac{m_\psi^2}{2}\psi^2 + \frac{\psi^4\phi^2 + \phi^4\psi^2}{8M'^2} \tag{41}$$

for what we will call model 1 and will be the primary focus of this work and

$$V = M^4 \cos^2(\phi/\sqrt{2}f) + \frac{m_\psi^2}{2}\psi^2 + \lambda^2\frac{\psi^2\phi^2}{4} \tag{42}$$

which we will call model 2.

The first model can be taken with M' at one of three regions: the Planck scale, the GUT scale or an intermediate scale ($\sim 10^{10}\ GeV$). At each scale the rest of the parameters are adjusted accordingly to produce sufficient inflation and agree with CMB data.

Quadratic Approximation	V_0	m_0	r	ψ_c	m_ψ
SUSY Model 1	M^4	$\frac{M^2}{\sqrt{2}f}$	4	$\frac{M\sqrt{2M'}}{\sqrt{f}}$	m_ψ
SUSY Model 2	M^4	$\frac{M^2}{\sqrt{2}f}$	2	$\frac{\sqrt{2}M^2}{f\lambda}$	m_ψ

TABLE I: Parameters of SUSY models and their counterparts in our quadratic approximation

We will approximate the potential with a pure quadratic one with a time varying waterfall mass, of the form

$$V(\phi, \psi) = V_0 - m_0^2 \left[1 - \left(\frac{\psi}{\psi_c} \right)^r \right] |\phi|^2 + m_\psi^2 \psi^2 \tag{43}$$

where $r = 4$ for model 1 and $r = 2$ for model 2, as can be easily seen by the form of the interaction terms in both cases. The correspondence between the exact SUSY potential and our quadratic counterpart is shown in Table I.

The parameters of the two models are restricted to fit CMB data, as shown in Fig. 3.

To lowest order, in this potential dominated model, the Hubble parameter is constant and equal to

$$H = \sqrt{\frac{8\pi}{3}} \frac{M^2}{M_p} = \sqrt{\frac{8\pi}{3}} \frac{\sqrt{V_0}}{M_p} \tag{44}$$

A.   End of Inflation

In our simplified quadratic model inflation will never end. The waterfall field will roll forever down its tachyonic potential. However, we shall not forget that this is a mere Taylor expansion of more realistic potentials, which have a well defined minimum. We will use the supersymmetric potentials of [5, 6] as a concrete example to connect our purely quadratic potential to ones with more realistic shapes. In these supersymmetric models the potential has a cosine-like form and the minimum occurs at $\frac{\phi}{\sqrt{2}f} = \frac{\pi}{2}$, where the inflaton will oscillate, terminating inflation and giving rise to (p)reheating. By making contact between the parameters of our potential and the physical parameters of the actual supersymmetric models, we can estimate the field value at which inflation ends.

There are two strategies for defining ϕ_{end}, the field value at which inflation ends. We can either pretend that the quadratic potential can be followed up to the end field value of the corresponding SUSY potential, or we can choose to end our calculation when the quadratic potential departs significantly from the actual SUSY potential that we are trying
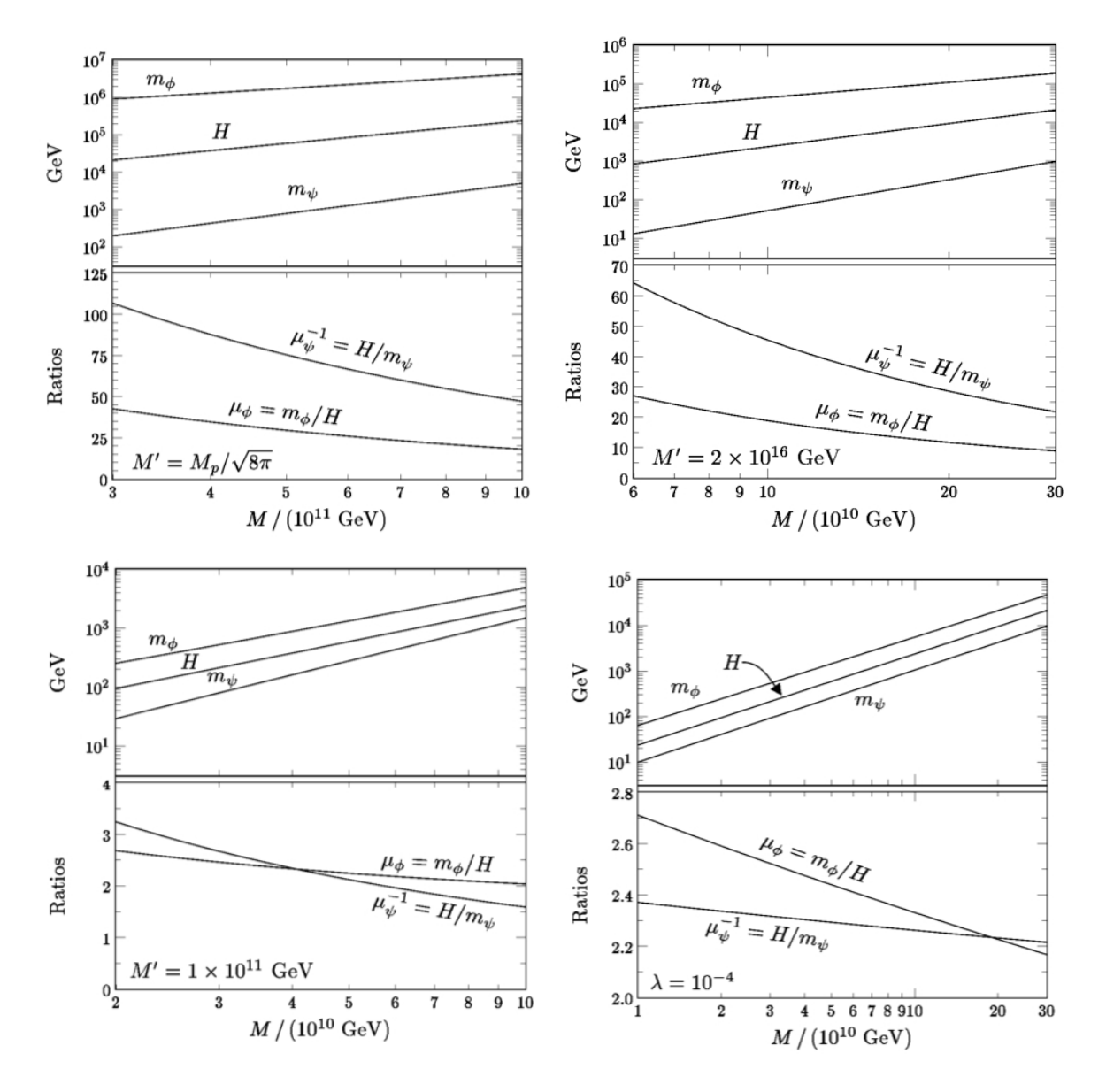
FIG. 3: Parameter space for the two supernatural inflation models. The bottom right corner shows the parameter for model 2, while the other three show parameters for model 1, for different ranges of the mass scale M'

to approximate.

In the first case the end field value is at $\phi_{\text{end}} = f\pi/\sqrt{2}$. To calculate the end field value for the latter case we will note that the cosine potential is accurately approximated by a quadratic as long as $\phi/f \ll 1$. We will call this ratio ϵ and in this case we will end our calculations when ϵ ceases being small. We can write these two cases in a unified manner,

as

$$\phi_{\text{end}} = \epsilon f \tag{45}$$

where $\epsilon = \pi/\sqrt{2}$ if we follow the quadratic potential all the way to the field value corresponding to the minimum of the SUSY potential and $\epsilon < 1$ if we stop our calculation at the point where the quadratic potential deviates significantly from the supersymmetric one.

Using the values of the parameters taken from the supersymmetric models, we can estimate the end field value to be

$$\phi_{\text{end}} \sim \epsilon \, 10^{15} H \tag{46}$$

within one or two orders of magnitude for all cases of models considered in [5, 6].

We will be using field values of this order of magnitude in our numerical calculations, whether we are dealing with the supersymmetric potentials or not. We will however examine the effects of changing the end value of the field and show that it is minimal, easily understandable, and calculable.

IV.   PERTURBATION THEORY BASICS

A.   Time delay formalism

The time delay formalism provides an intuitive and straightforward way to calculate primordial perturbations. Its basic principle is that inflation ends at different places in time at different times, due to quantum fluctuations. This leads some of the regions of the universe to have inflated more than others, creating a difference in their densities. The time-delay formalism was first introduced by Hawking [24] and by Guth and Pi [25], and has recently been reviewed in Ref. [26].

We will briefly describe the method here for the case of a single real scalar field. The universe is assumed to be described by a de-Sitter space-time, since the Hubble parameter is taken to be a constant. The equation of motion for the scalar field $\phi(\vec{x}, t)$ is

$$\ddot{\phi} + 3H\dot{\phi} = -\frac{\partial V}{\partial \phi} + \frac{1}{a(t)^2}\nabla^2\phi \tag{47}$$

where the last term is suppressed by an exponentially growing quantity, so at late times it becomes negligible. We will omit the last term from now on.

We call the homogenous (classical) solution $\phi_0(t)$ and write the full solution, including a space dependent small perturbation $\delta\phi \ll \phi_0$ as

$$\phi(\vec{x}, t) = \phi_0(t) + \delta\phi(\vec{x}, t) \tag{48}$$

Plugging this into the equation of motion and working to linear order in $\delta\phi$ one can show that the quantity $\delta\phi$ obeys the same differential equation as $\dot{\phi}_0$. Furthermore the presence of a damping term implies that any two solutions approach a time independent ratio at large times. Thus, at large times we have (to first order in $\delta\tau$)

$$\delta\phi(\vec{x}, t) \to -\delta\tau(\vec{x})\dot{\phi}_0(t) \Rightarrow \phi(\vec{x}, t) \to \phi_0(t - \delta\tau(\vec{x})) \tag{49}$$

This is the formulation of the intuitive picture of the time delay method.

B.   Randall-Soljacic-Guth approximation

The usual calculation of density perturbations in inflation considers small quantum fluctuations around a classical field trajectory. In the case of hybrid inflation such a classical trajectory does not exist, since classically the field would stay forever on the top of the inverted potential. It is the quantum fluctuations that push the field away from this point of unstable equilibrium. One way to overcome this difficulty is to consider the RMS value of the field as the classical trajectory. This was done for example in [5] and [6] and is a recurring approximation in the study of hybrid inflation.

Using the Bunch-Davies vacuum in the definition of the RMS value of the waterfall field $\phi_{\rm rms} = \sqrt{\langle 0|\phi(x,t)\phi^*(x,t)|0\rangle}$ it it straightforward to calculate it using the mode expansion

$$\phi_{\rm rms}^2(t) = \frac{1}{b^3} \sum_{\vec{k}, \vec{k}'} e^{i(\vec{k}-\vec{k}')\cdot x} \left\langle 0|(c_{\vec{k}}u_{\vec{k}} + d^\dagger_{-\vec{k}}u^*_{-\vec{k}})(c^\dagger_{\vec{k}'}u^*_{\vec{k}'} + d_{-\vec{k}'}u_{-\vec{k}'})|0 \right\rangle = \frac{1}{b^3} \sum_{\vec{k}} |u_k(t)|^2 \tag{50}$$

The mean fluctuations are measured by

$$\Delta\phi(\vec{k}) = \left[\left(\frac{k}{2\pi}\right)^3 \int d^3x \, e^{i\vec{k}\cdot\vec{x}} \langle\phi(x)\phi^*(0)\rangle \right]^{1/2} = \left[\left(\frac{k}{2\pi}\right)^3 |u_{\vec{k}}|^2 \right]^{1/2} \tag{51}$$

resulting in what will be called the RSG approximation for the time delay field

$$\Delta\tau_{RSG}(\vec{k}) \approx \frac{\Delta\phi(\vec{k}, t)}{\dot{\phi}_{\rm rms}} = \left(\frac{kb}{2\pi}\right)^{3/2} |u_{\vec{k}}| \frac{\sqrt{\sum_{\vec{k}} |u_{\vec{k}}(t)|^2}}{\sum_{\vec{k}} \dot{u}_{\vec{k}}(t)u_{\vec{k}}(t)} \tag{52}$$
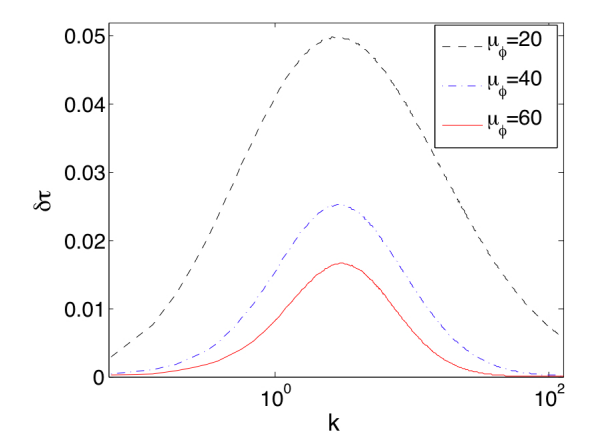
FIG. 4: The time delay field calculated using the RSG formalism. The end time was taken to be 15 e-folds after the waterfall transition and $\mu_\psi = \frac{1}{20}$ for all curves, while we varied μ_ϕ.

There is an important comment to be made about the quantum mechanical nature of these density perturbations. In regular models of inflation quantum perturbations are scaled by $\hbar$. We can think of them as modes with initial conditions that are of the order of $\hbar$. The classical trajectory on the other hand does not have any quantum mechanical origin, hence does not scale with $\hbar$. This means that in the limit of $\hbar \to 0$ the perturbations vanish, as one would expect will happen if one could "switch off" quantum mechanical effects.

In the case of hybrid inflation on the other hand, what we call the classical trajectory (be it the RMS value or something else) is comprised of modes that originated as quantum fluctuations, hence is scaled by $\hbar$ itself. This means that even in the limit of $\hbar \to 0$, the density perturbations in hybrid inflation remain finite! By explicitly restoring $\hbar$ in the formulas of the paper, the reader can formally arrive to the same conclusion.

Some plots of the time delay field calculated using the RSG approximation are shown in Fig. 4. The reduced mass of the timer field was taken to be $\mu_\psi = \frac{1}{20}$ while we varied the waterfall field mass. We fixed the time at which inflation ended to be 15 e-folds after the waterfall transition.

V. CALCULATION OF THE TIME DELAY POWER SPECTRUM

The usual method to calculate the primordial perturbation spectrum would involve either making some approximations (more or less similar to the RSG) or using a Monte Carlo

simulation. The former suffers from the lack of a classical trajectory that invalidates the usual perturbation method, while the latter would be computationally costly in three spatial dimensions. We will therefore implement an alternate method that reduces the calculation of the spectrum of the time delay field to the evaluation of a two dimensional integral and does not need a classical trajectory to do so.

As discussed at the end of Sec. II D 3, the behavior of the mode functions at asymptotically late times $(t \to \infty)$ is given by

$$u(\vec{k}, t \to \infty) \sim e^{\lambda_0 t} u(\vec{k}) \; , \tag{53}$$

where λ_0 is given by Eq. (40). If we define for all times

$$\lambda(t) \equiv \frac{\dot{\phi}_{\rm rms}(t)}{\phi_{\rm rms}(t)} = \frac{\sum_{\vec{k}} \frac{R(\vec{k},t)\dot{R}(\vec{k},t)}{2|k|}}{\sum_{\vec{k}} \frac{|R(\vec{k},t)|^2}{2|k|}} \; , \tag{54}$$

then at late times $\lambda(t) \to \lambda_0$. Since $\lambda(t)$ changes very slowly, we can take it as a constant around the time of interest.

To discuss fluctuations in the time at which inflation ends, we begin by defining t_0 as the time when the rms field reaches the value $\phi_{\rm end}$, which we have chosen to define the nominal end of inflation:

$$\phi_{\rm rms}^2(t_0) = \phi_{\rm end}^2 \; . \tag{55}$$

Since at late times all modes, to a good approximation, grow at the same exponential rate $\lambda(t)$, we can express the field $\phi(\vec{x}, t)$ at time $t = t_0 + \delta t$ in terms of the field $\phi(\vec{x}, t_0)$ by

$$|\phi(\vec{x}, t)|^2 = |\phi(\vec{x}, t_0)|^2 e^{2\lambda \delta t} \; . \tag{56}$$

If t is chosen to be the time $t_{\rm end}(\vec{x})$ at which inflation ends at each point in space, then $\phi(\vec{x}, t_{\rm end}(\vec{x})) = \phi_{\rm end} = \phi_{\rm rms}(t_0)$, and the above equation becomes

$$\phi_{\rm rms}^2(t_0) = |\phi(\vec{x}, t_0)|^2 e^{2\lambda \delta t} \; , \tag{57}$$

which can be solved for the time delay field $\delta t(\vec{x}) = t_{\rm end}(\vec{x}) - t_0$:

$$\delta t(\vec{x}) = \frac{-1}{2\lambda} \log \left(\frac{|\phi(\vec{x}, t_0)|^2}{\phi_{\rm rms}^2(t_0)} \right) \; . \tag{58}$$

Rescaling by the rms field

$$\tilde{\phi}(\vec{x}, t) \equiv \frac{\phi(\vec{x}, t)}{\phi_{\rm rms}(t)} \; , \tag{59}$$

we can write

$$\delta t(\vec{x}) = \frac{-1}{2\lambda} \log |\tilde{\phi}(\vec{x}, t_0)|^2 \; . \tag{60}$$

Using this expression, we can write the two-point function of the time delay field as

$$\left\langle \delta t(\vec{x}) \delta t(\vec{0}) \right\rangle = \frac{1}{4\lambda^2} \left\langle \log |\tilde{\phi}(\vec{x}, t_0)|^2 \log |\tilde{\phi}(\vec{0}, t_0)|^2 \right\rangle \; , \tag{61}$$

which can be evaluated, since the probability distributions are known. To continue, we can decompose the complex scalar field in terms of the real fields X_i:

$$\tilde{\phi}(\vec{x}, t) = X_1 + iX_2 \;\; , \;\; \tilde{\phi}(\vec{0}, t) = X_3 + iX_4 \; . \tag{62}$$

The average value of a function F of a random variable X with probability distribution function $p(X)$ is given by

$$\langle F[X] \rangle = \int dX p(X) F[X] \; . \tag{63}$$

Since this is a free field theory, we can take the four random variables $X_i(\vec{x})$ to follow a joint Gaussian distribution with

$$p(X) = \frac{1}{(2\pi)^2 \sqrt{\det(\Sigma)}} \exp\left(-\frac{1}{2} X^T \Sigma^{-1} X\right) \;\; , \;\; \Sigma_{ij} = \langle X_i X_j \rangle \; . \tag{64}$$

A function of the $X_i's$ then has the expected value

$$\langle F[X] \rangle = \int \prod_{i=1}^4 dX_i \frac{1}{(2\pi)^2 \sqrt{\det(\Sigma)}} \exp\left(-\frac{1}{2} X^T \Sigma^{-1} X\right) F[X] \; . \tag{65}$$

The new fields X_i can be written in terms of the original complex field ϕ as

$$\begin{aligned} X_1 &= \frac{1}{2}\left[\tilde{\phi}(\vec{x}) + \tilde{\phi}^*(\vec{x})\right] \;\; , \;\; X_2 = \frac{1}{2i}\left[\tilde{\phi}(\vec{x}) - \tilde{\phi}^*(\vec{x})\right] \\ X_3 &= \frac{1}{2}\left[\tilde{\phi}(\vec{0}) + \tilde{\phi}^*(\vec{0})\right] \;\; , \;\; X_4 = \frac{1}{2i}\left[\tilde{\phi}(\vec{0}) - \tilde{\phi}^*(\vec{0})\right] \end{aligned} \tag{66}$$

The components of the variance matrix Σ can be easily calculated using the commutation relations for the creation and annihilation operators in $\phi(\vec{x}, t)$, from Eq. (16). Due to the high degree of symmetry the matrix itself has a very simple structure:

$$\Sigma = \begin{pmatrix} \frac{1}{2} & 0 & \Delta & 0 \\ 0 & \frac{1}{2} & 0 & \Delta \\ \Delta & 0 & \frac{1}{2} & 0 \\ 0 & \Delta & 0 & \frac{1}{2} \end{pmatrix} \; , \tag{67}$$

where

$$\Delta(\vec{x}, t_0) = \langle X_1 X_3 \rangle = \langle X_2 X_4 \rangle = \frac{1}{2} \left\langle \phi^*(\vec{x}, t_0)\phi(\vec{0}, t_0) \right\rangle = \frac{1}{2b^3} \sum_{\vec{k}} |\tilde{u}(\vec{k}, t_0)|^2 e^{i\vec{k}\cdot\vec{x}} , \tag{68}$$

where

$$\tilde{u}(\vec{k}, t) = \frac{u(\vec{k}, t)}{\phi_{\rm rms}(t)} . \tag{69}$$

Since $\tilde{u}(\vec{k}, t)$ actually depends only on the magnitude of the wavenumber, because of the isotropy of the problem, we can do the angular calculations explicitly in Δ and leave only the radial integral to be calculated numerically. Then

$$\left\langle \delta t(\vec{x})\delta t(\vec{0}) \right\rangle = \frac{1}{4\lambda^2} \frac{1}{(2\pi)^2[\frac{1}{4} - \Delta^2]} \int dX_1 dX_2 dX_3 dX_4 \log(X_1^2 + X_2^2) \log(X_3^2 + X_4^2)$$
$$\times \exp\left\{ -\frac{1}{4[\frac{1}{4} - \Delta^2]} \left[X_1^2 + X_2^2 + X_3^2 + X_4^2 - 4(X_1 X_3 + X_2 X_4)\Delta \right] \right\} . \tag{70}$$

Changing to polar coordinates

$$X_1 = r_1 \cos\theta_1 , \ X_2 = r_1 \sin\theta_1$$
$$X_3 = r_2 \cos\theta_2 , \ X_4 = r_2 \sin\theta_2 , \tag{71}$$

the integral becomes

$$\left\langle \delta t(\vec{x})\delta t(\vec{0}) \right\rangle = \frac{2}{\pi\lambda^2(1 - 4\Delta^2)} \int_0^{2\pi} d\theta \int_0^\infty r_1 dr_1 \int_0^\infty r_2 dr_2 \log(r_1) \log(r_2)$$
$$\times \exp\left[-\frac{r_1^2 + r_2^2 - 4\Delta r_1 r_2 \cos\theta}{1 - 4\Delta^2} \right] , \tag{72}$$

where we redefined the angular variables as $\theta = \theta_1 - \theta_2$ and $\tilde{\theta} = \theta_1 + \theta_2$ and integrated over $\tilde{\theta}$. Changing also the radial variables

$$r_1 = r \cos\phi , \ r_2 = r \sin\phi , \tag{73}$$

$$\left\langle \delta t(\vec{x})\delta t(\vec{0}) \right\rangle = \frac{1}{\pi\lambda^2(1 - 4\Delta^2)} \int_0^{2\pi} d\theta \int_0^{\frac{\pi}{2}} d\phi \, \sin 2\phi \int_0^\infty dr \, r^3 \log(r \cos\phi) \log(r \sin\phi)$$
$$\times \exp\left[-\frac{(1 - 2\Delta \sin 2\phi \cos\theta) r^2}{1 - 4\Delta^2} \right] . \tag{74}$$

The radial integration can be performed analytically

$$\int_0^\infty dr \, r^3 \, \log(ar) \log(br) e^{-cr^2} = \tag{75}$$
$$\frac{1}{8c^2} \left[(\gamma - 2)\gamma + \frac{\pi^2}{6} - 2\log(ab)(\gamma - 1 + \log(c)) + 4\log(a)\log(b) + \log(c)(2\gamma - 2 + \log(c)) \right]$$

where $a = \cos\phi$, $b = \sin\phi$, $c = \frac{1}{(1-4\Delta^2)}(1 - 2\Delta\sin 2\phi\cos\theta)$ and γ is the Euler constant $\gamma \approx 0.57721$.

Finally, the spectrum of the time delay field is defined by

$$\delta\tau(\vec{k}) = \left[\left(\frac{k}{2\pi}\right)^3 \int d^3x\, e^{i\vec{k}\cdot\vec{x}}\left\langle\delta t(\vec{x})\delta t(\vec{0})\right\rangle\right]^{1/2}. \tag{76}$$

Calculation in the two limiting cases $x \to 0$ and $x \to \infty$ (or $x \to b$ in our case) can be done analytically.

1. For $x \to 0$ several terms in the integral diverge, since $\Delta \to \frac{1}{2}$. In this case we have only two degrees of freedom instead of four, since we consider a complex scalar field at one point in space. The integral becomes

$$\left\langle\delta t(\vec{0})\delta t(\vec{0})\right\rangle = \frac{1}{4\lambda^2}\int\frac{dX_1 dX_2}{\pi}e^{-(X_1^2+X_2^2)}\log^2(X_1^2+X_2^2) =$$
$$= \frac{1}{4\pi\lambda^2}\int_0^{2\pi}d\theta\int_0^\infty dr\, re^{-r^2}\log^2(r^2) = \frac{1}{4\lambda^2}\left(\gamma^2 + \frac{\pi^2}{6}\right). \tag{77}$$

2. The $x \to \infty$ limit is much easier to handle. We recognize that $\Delta(\vec{x})$ is simply the Fourier transform of $|u_k|^2$. Since u_k is smooth, $\Delta(x \to \infty) \to 0$, and therefore $\delta t(\infty)$ is uncorrelated with $\delta t(\vec{0})$. Eq. (70) can be seen to factorize, giving $\left\langle\delta t(\infty)\delta t(\vec{0})\right\rangle = \left\langle\delta t(\vec{0})\right\rangle^2$, where

$$\left\langle\delta t(\vec{0})\right\rangle = \frac{-1}{2\pi\lambda}\int dX_1 dX_2\log(X_1^2+X_2^2)\exp\left[-(X_1^2+X_2^2)\right]$$
$$= -\frac{1}{\pi\lambda}\int_0^{2\pi}d\theta\int_0^\infty r\,dr\,\log r e^{-r^2}$$
$$= \frac{\gamma}{2\lambda}. \tag{78}$$

Combining these results, we see that the probability distribution for $\delta t(\vec{0})$ has a standard deviation $\sigma = \sqrt{\left\langle\delta t(\vec{0})^2\right\rangle - \left\langle\delta t(\vec{0})\right\rangle^2} = \pi/(2\sqrt{6}\lambda)$. While the first limit above is needed for programming the numerical calculations, since the integral of Eq. (70) cannot be numerically evaluated at $\vec{x} = \vec{0}$, the second limit can be used as a numerical check.

The same method can be applied to the exact calculation of any higher order correlation functions. Especially the non-Gaussian part of the power spectrum f_{NL} can be read off from the momentum space Fourier transform of the three-point correlation function in position space $\langle\delta t(\vec{x}_1)\delta t(\vec{x}_2)\delta t(x_3)\rangle = \langle\delta t(\vec{x}_1)\delta t(\vec{x}_2)\delta t(0)\rangle$. Taking the Fourier transform we can compute $\left\langle\delta t(\vec{k}_1)\delta t(\vec{k}_2)\delta t(k_3)\right\rangle$, from which we can extract the properties of the bispectrum.

The form of the three point function in position space is

$$\langle \delta t(\vec{x}_1)\delta t(\vec{x}_2)\delta t(0)\rangle = \frac{-(2\pi)^2}{\lambda^3}\int_0^{2\pi} d\gamma_1 d\gamma_2 \int_0^{\pi}\sin\theta d\theta \int_0^{2\pi} d\phi F(\gamma_1,\gamma_2,\theta,\phi) \tag{79}$$

where $F(\gamma_1,\gamma_2,\theta,\phi)$ is a function of four angular variables. Calculations regarding the form of the bispectrum will be published elsewhere.

VI. NUMERICAL RESULTS AND DISCUSSION

Let us begin by plotting one example of the free field theory (FFT) calculation of the time delay power spectrum, from Eqs. (74) and (76), along with the corresponding curve derived using the RSG approximation, Eq. (52). We use the sample parameters $\mu_\psi = \frac{1}{20}$ and $\mu_\phi = 20$. Both calculations give a spike, but a spike of different width, different height and different position. Let us rescale the RSG result as follows

$$\delta\tau_{\text{RSG,rescaled}}(k) = A\,\delta\tau_{\text{RSG}}\left(Bk\right), \tag{80}$$

where A and B are $O(1)$ constants calculated by requiring the peaks of the FFT and RSG distributions to match in position and amplitude. The results are plotted in Fig. 5. We can see that the FFT and RSG curves do not seem similar. However the rescaled RSG curve seems to follow the FFT curve very well, as was first noticed by Burgess [13]. Based on our simulations the curves generally tend to agree better for low wavenumbers, up to and including the peak, and start deviating after the peak. The rescaling parameters vary with the field masses chosen and for the particular choice of Fig. 5 were calculated to be $A = 0.6152$ and $B = 3.25$. We do not yet fully understand this behavior, but we are studying it both analytically and numerically and will present our findings in a subsequent paper.

We will now do an extensive scan of parameter space $\{\mu_\phi, \mu_\psi\}$ in order to have reliable estimates on the magnitude and wavelength of the perturbations. This is important both to make sure that CMB constraints can be satisfied as well as to study the formation of primordial black holes that might lead to the supermassive black holes found in the centers of galaxies. Since the original motivation for this paper has been the supersymmetric models first presented in [5] and [6], we will present the results for the perturbations in these models. However, our quadratic approximation holds for more general hybrid inflation models. Hence
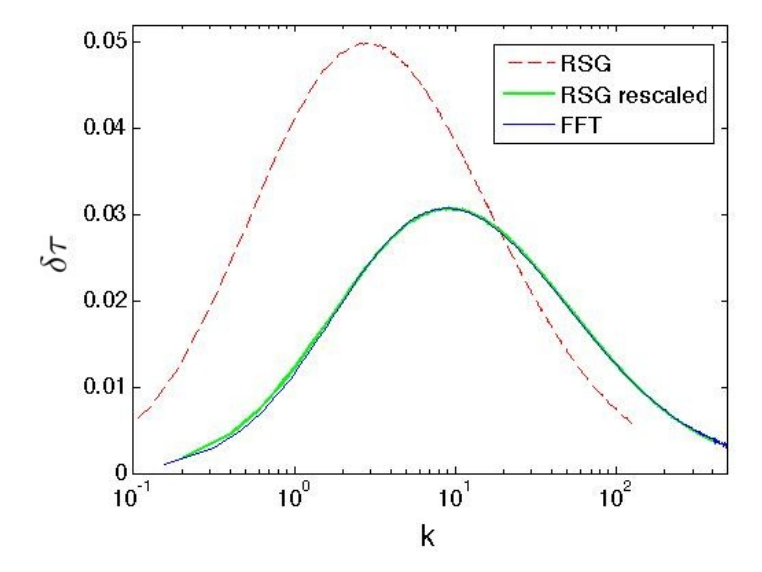
FIG. 5: Comparison between the RSG and FFT methods. The end time was taken to be 15 e-folds after the waterfall transition and $\mu_\phi = 20$ and $\mu_\psi = 1/20$. We can see that the spectrum of the time delay field calculated in the free field theory agrees very well with the rescaled version of the RSG approximation $A\,\delta\tau_{RSG}\,(Bk)$.

it is important to make a model-independent parameter sweep. This will provide a more general set of predictions of this class of models. We will give both exact power spectra, as well as try to isolate the dominant features and provide a qualitative understanding of their dependence on the model's parameters.

A. Model-Independent Parameter Sweep

There are several model-dependent parameters that give us some control over the properties of the resulting power spectrum. Initially we will fix the value of the field at the end of inflation to be $|\phi_{\text{end}}| = 10^{14}$ in units of the Hubble parameter. With this assumption (which will be relaxed later), we can calculate the properties of the power spectrum as a function of the masses. Initially we fix the reduced timer field mass to be $\mu_\psi = \frac{1}{20}$ and vary the mass of the waterfall field. The results are shown in Fig. 6. We have plotted (clockwise from the top left)

1. The end time of inflation, defined as the time when the RMS value of the field reaches the end value.
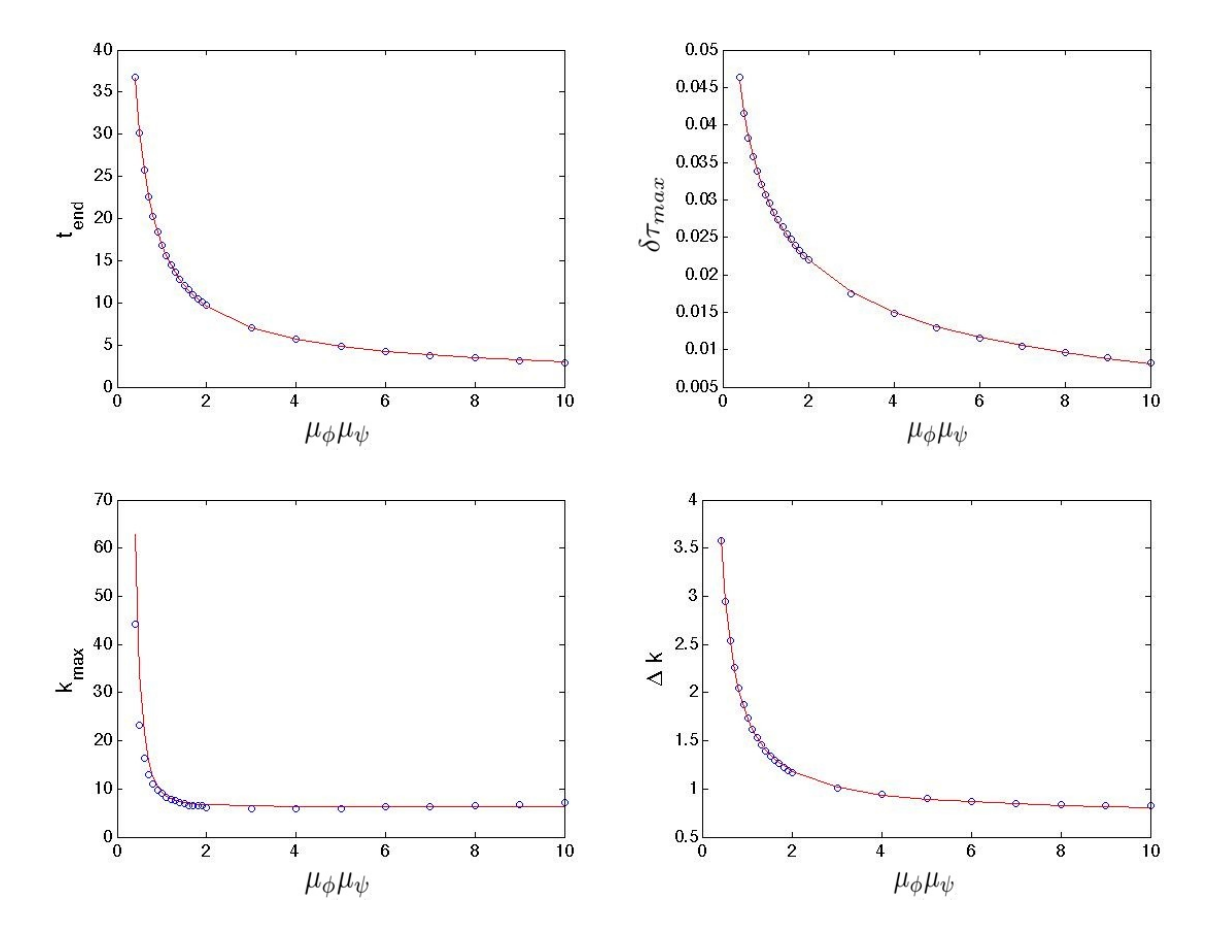
FIG. 6: Parameter sweep for constant timer field mass $\mu_\psi = 1/20$ and constant end field value $\phi_{\text{end}} = 10^{14}$. Data points are plotted along with a least square power law fit. The same trend is evident in all curves. The time delay spectrum grows in amplitude and width and is shifted towards larger momentum values as the mass product decreases. Also inflation takes longer to end for low mass product.

2. The maximum amplitude of the spectrum of the time delay.

3. The comoving wavenumber at which the aforementioned maximum value occurs. Thinking about black holes, this is the scale at which black holes will be most likely produced.

4. The width of the time delay distribution in the logarithmic scale, taken as $\Delta k = \log_{10}\left(\frac{k_{+1/2}}{k_{-1/2}}\right)$ where $k_{\pm 1/2}$ are the wavenumbers at which the distribution reaches one half of its maximum value.
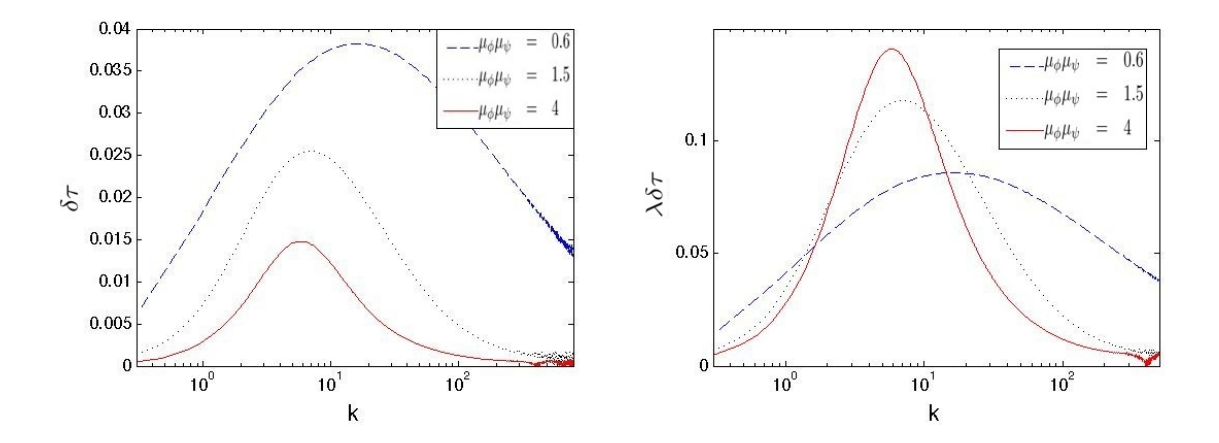
FIG. 7: Time delay spectra for different values of the mass product, keeping the timer field mass fixed at $\mu_\psi = \frac{1}{20}$

We see that all the plotted quantities show a decreasing behavior as one increases the mass product. In order to quantify this statement, we fitted each set of data points with a power law curve of the form $y = ax^b + c$. The scaling exponent b for the various quantities was $b_{t_{\text{end}}} \approx -0.88$, $b_{\delta\tau_{max}} \approx -0.34$, $b_{kmax} \approx -3.219$, $b_{\Delta k} \approx -1.17$. As a comparison, the corresponding best fit exponent of the growth rate λ as a function of the mass product is $b_\lambda \approx -0.85$.

In order to get a better understanding of what these parameters actually mean, we plot three characteristic spectra for three values of the mass ratio in Fig. 7. We also rescale the spectra by the growth factor λ. This probes the actual form of the two point correlation function, as seen in momentum space. That is, it shows the evaluation of the spectrum in Eq. (76), while ignoring the factor of $1/\lambda^2$ in the evaluation of $\left\langle \delta t(\vec{x})\delta t(\vec{0}) \right\rangle$ from Eq. (74).

Before continuing to a more thorough examination of parameter space, let us understand how changing the field value at the end of inflation will change our results. Fixing the product of the reduced masses equal to 2 ($\mu_\psi = \frac{1}{20}$ and $\mu_\phi = 40$), we let the field value ϕ_{end} vary by four orders of magnitude. The results are shown in Fig. 8. It is evident that the curves for $\delta\tau(k)$ are of identical form and slightly different magnitude. The last graph shows the product $\lambda \cdot \delta\tau(k)$ for the two curves at $\phi_{\text{end}} = 10^{12}$ and $\phi_{\text{end}} = 10^{16}$, plotted respectively as a green thick and a black thin line. It is seen, that once rescaled the two curves fall exactly on top of each other, meaning that the actual integral that gives us the two point function in position space is time independent, once we enter the region where
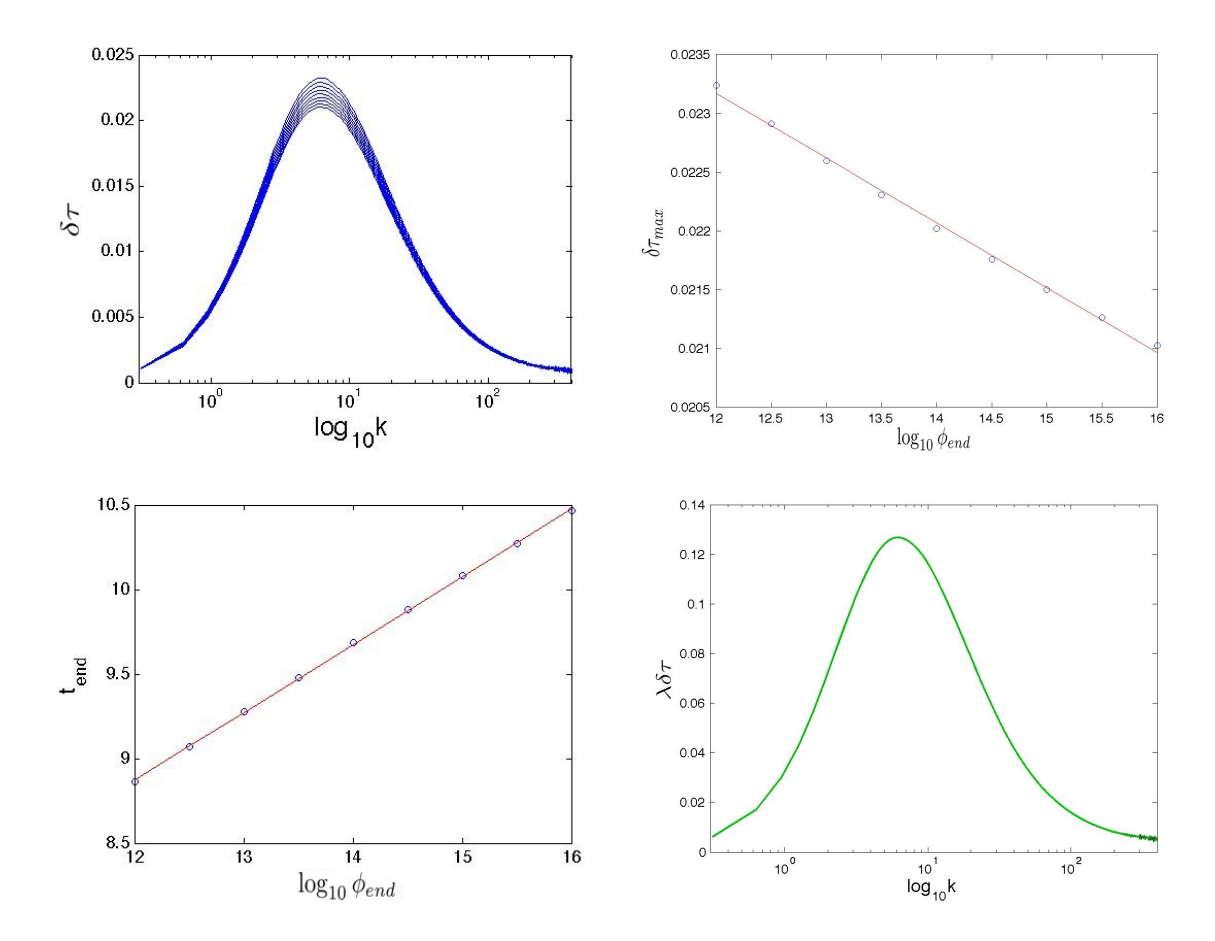
FIG. 8: Perturbation spectrum for varying field value at t_{end} for constant masses. The time delay curves are identical in shape and differ only in amplitude. This variation is entirely due to the different value of the time dependent growth factor λ, which differs for each case because inflation simply takes longer to end for larger end field values.

all modes behave identically. Furthermore if one takes the product of the maximum value of the time delay times the growth parameter ($\delta\tau_{max} \cdot \lambda$) for the different values of ϕ_{end} the result is constant for the range explored here to better than 1 part in 10^6, meaning that they are identical within the margins of numerical error. Thus, changing the value of the field at which inflation ends can affect the resulting perturbation spectrum only by changing the growth parameter λ, for which we have a very accurate analytical estimate in the form of Eq. (39). From this point onward, we will keep the end field value fixed at $\phi_{\mathrm{end}} = 10^{14}$ and keep in mind that the fluctuation magnitude can change by 10% or so if this field value changes.

Once we fix the field magnitude at the end of inflation we have two more parameters to vary, namely the two masses: the actual timer field mass and the asymptotic tachyonic waterfall field mass. The two masses can be varied either independently on a two dimensional plane or along some line on the plane, in a specific one-dimensional way. Fixing one of the two masses is such a way of dimensional reduction of the available parameter space, as we did before. Another way to eliminate one of the variables is to fix the mass product and change the mass ratio. This will prove and quantify the statement, that (at least for heavy waterfall and light timer fields) the result is controlled primarily by the mass product.

We fix the mass product at $\mu_\phi \mu_\psi = 2$. The results are shown in Fig. 9. The curves are of identical form and everything is again controlled only by λ. On the top left figure we plotted $\lambda \, \delta\tau$ for the two extreme values and the curves fall identically on top of each other (color-coding is as before). Furthermore if we calculate the product $\lambda \cdot \delta\tau_{max}$ for different values of the mass ratio we get a constant result $0.1225 \pm 2 \cdot 10^{-5}$ where the discrepancy can be attributed to our finite numerical accuracy. The second feature of this calculation is the extremely flat part of the end-time, growth factor and maximum time delay curves for large values of the mass ratio and the abrupt change as the mass ratio gets smaller. For the value of the mass product that we have chosen, this transition happens as the timer field mass approaches unity. Let us look at the expansion of the effective waterfall field mass

$$\mu_{\phi,eff}^2 = \mu_\phi^2 \left(1 - e^{-\tilde{\mu}_\psi^2 N} \right) = \mu_\phi^2 \tilde{\mu}_\psi^2 N (1 - \tilde{\mu}_\psi^2 N + ...) \tag{81}$$

When the second term in the expansion cannot be neglected, the dynamics of the problem stops being defined by the mass product alone. This explains the abrupt change we see as we lower the mass ratio. By doing the same simulation for different values of the fixed mass product we get similar results.

We can now do the opposite, that is fix the ratio and change the mass product. The results are shown as the open circles in the top two diagrams of Fig. 10, and in the lower diagrams of the figure. There are two main comments to be made. First of all, in the case of a fixed ratio, the growth rate λ does not solely determine the results. Rescaling the spectrum by λ not only fails to give a constant peak amplitude (Fig. 10, lower left), but the result are spectra of different shapes (Fig. 10, lower right). On the other hand, the data points taken with a constant mass ratio and a constant timer field mass ($\mu_\psi = \frac{1}{20}$), as shown by the +'s on the upper diagrams of Fig. 10, fall precisely on the same curve! This clearly
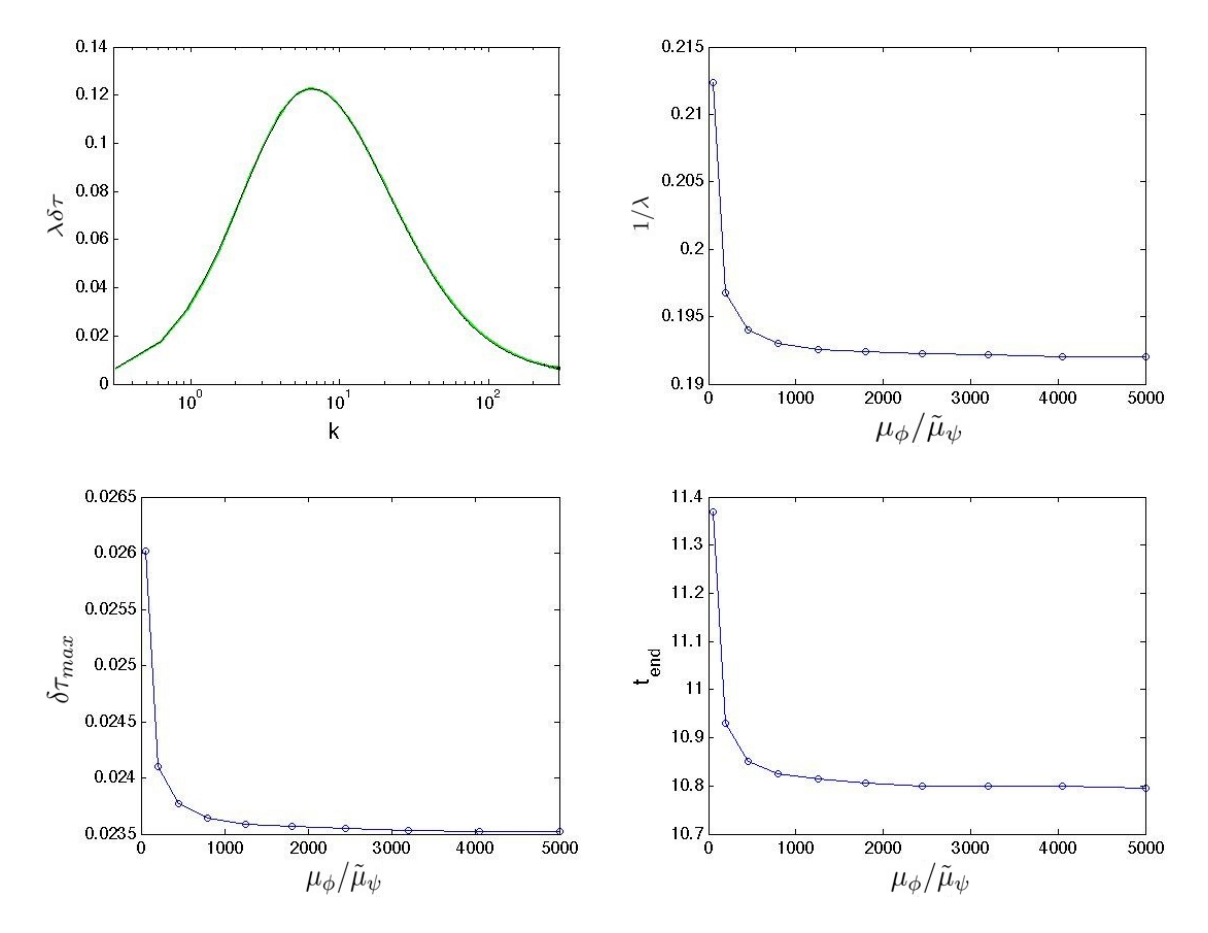
FIG. 9: Fixing the mass product at 2 and varying the mass ratio. There is significant variation only for low mass ratio, when the light timer field approximation loses its validity. Furthermore the curves of maximum time delay amplitude and $1/\lambda$ follow each other exactly up to our numerical accuracy. Finally by rescaling the spectra by the growth factor λ they become identical for all values of the mass ratio.

demonstrates that the only relevant parameter, at least for a light timer field, is the mass product!

We see that contrary to the fixed product case, the results for fixed mass ratio do not depend solely on λ. We have established that the the most important factor in determining the time delay field is the product of the waterfall and timer field masses, especially for a light timer field.
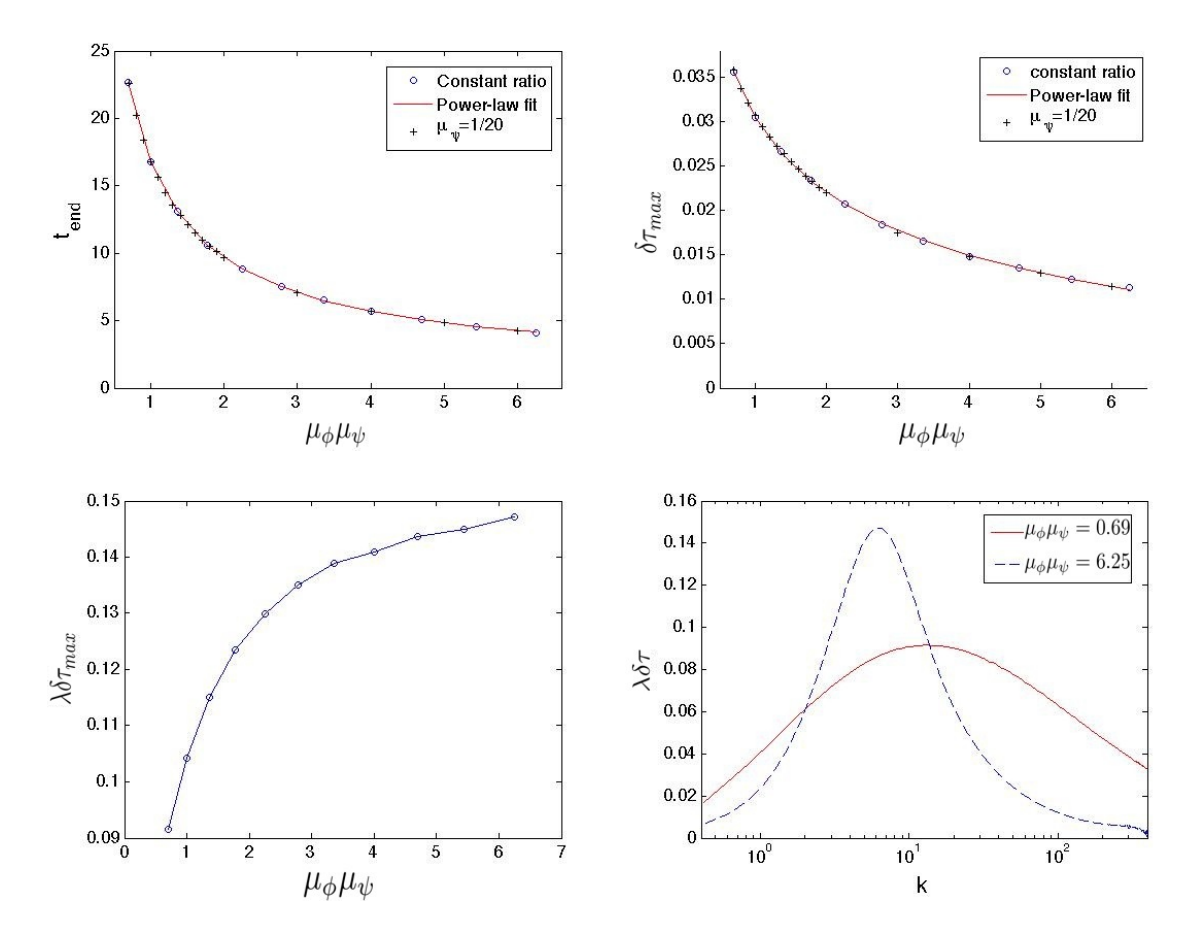
FIG. 10: Fixing the mass ratio at 900 (open circles) or the timer mass at $\mu_\psi = 1/20$ (+'s). The time delay spectra for different mass products show no common shape characteristics and remain different even when rescaled by λ. Furthermore the end time and maximum perturbation amplitude curves are identical for constant mass ratio and constant timer field mass, proving that indeed the mass product is the dominant parameter.

B.   Supernatural Inflation

We now turn our attention to the supernatural inflation models that were studied in [5] and [6]. We will examine each of the four cases separately.

Let us start with the first SUSY model (described by Eq. (41)) with the interaction-suppressing mass scale M' set at the Planck scale. The mass of the timer field was calculated to be 50 to 100 times less than the Hubble scale, while the asymptotic waterfall field mass was more than 20 times the Hubble scale. This means that the model is well into the region where the two masses are separated by a few orders of magnitude. According to the analysis of the previous section, we expect the mass product to be the dominant factor in
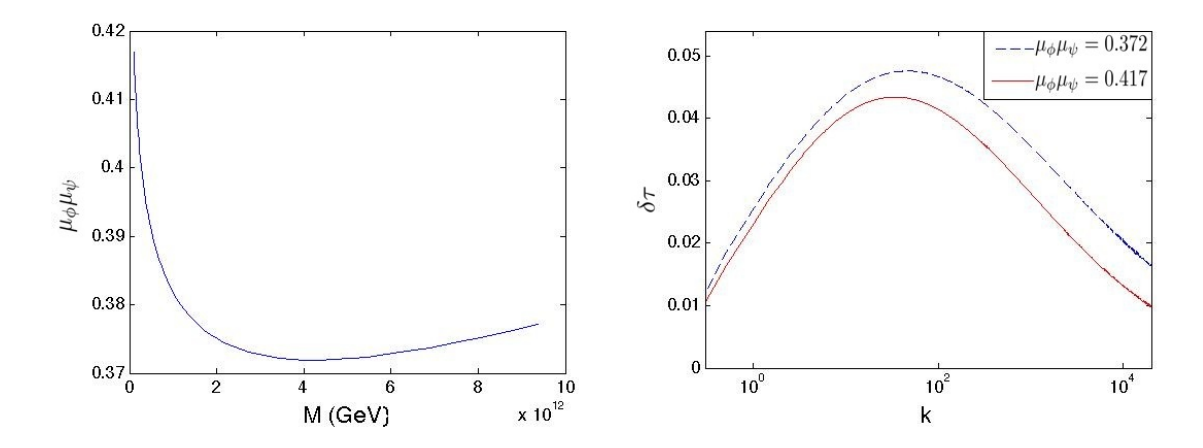
FIG. 11: First Supernatural inflation model with M' at the Planck scale. The spectra corresponding to the maximum and minimum mass product are shown. We observe good agreement with the results of the model independent parameter sweep of the previous section, because the timer field mass is much smaller than the Hubble scale.

the generation of density perturbations. In the left part of Fig. 11 we see the mass product for this model. We can see that the mass product varies less than 15%. It is hence enough to calculate the time delay spectra for the two extreme values and say that all other values of the mass product will fall between the two, as shown in 11.

Putting the mass scale M' of the first SUSY model at the GUT scale changes the masses as well as the Hubble scale by one order of magnitude. However the reduced masses and their product have very similar values as before. This is shown in Fig. 12

It is worth noting that these two SUSY models contain a very light timer field, hence the results should be the same as our previous parameter space sweep with a constant light timer field. If one compares Fig. 11 and Fig. 12 with Fig. 6, we indeed see excellent agreement for the amplitude and width of the time delay spectrum.

When setting the mass scale M' at some lower scale of 10^{11} GeV, the reduced timer and waterfall masses become $O(1)$. This means that in this case the parameter λ saturates faster and the perturbation spectrum reaches its asymptotic limit earlier and becomes time-independent from that point onward. Furthermore the actual value of the growth parameter λ is smaller, leading to an enhanced perturbation amplitude, the largest among the models studied here. The mass product changes by a factor of 2.5 as seen in Fig. 13. We choose five points in the allowed interval of mass values and calculate the corresponding curves. The specific values of the mass parame-
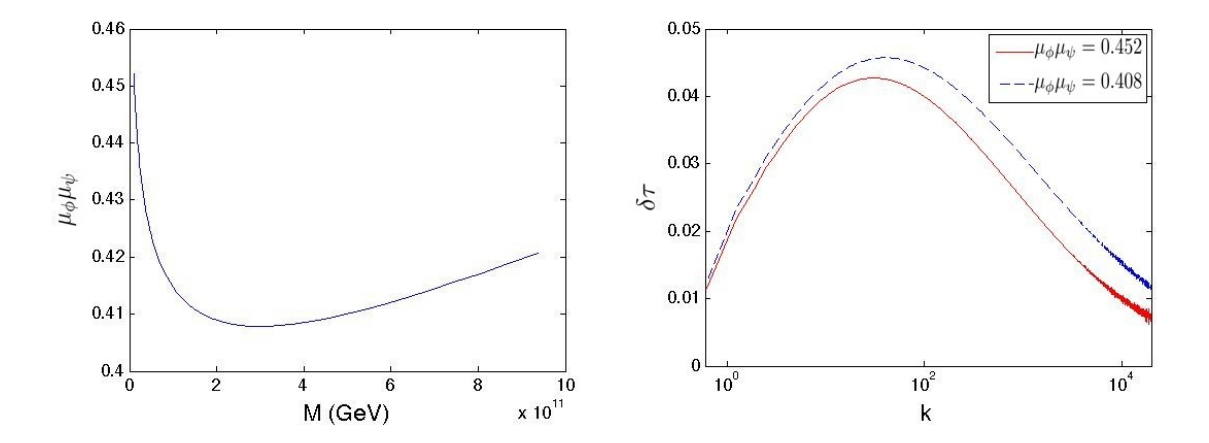
FIG. 12: First Supernatural inflation model with M' at the GUT scale. The spectra corresponding to the maximum and minimum mass product are shown. There is again good agreement with the results of the previous section.
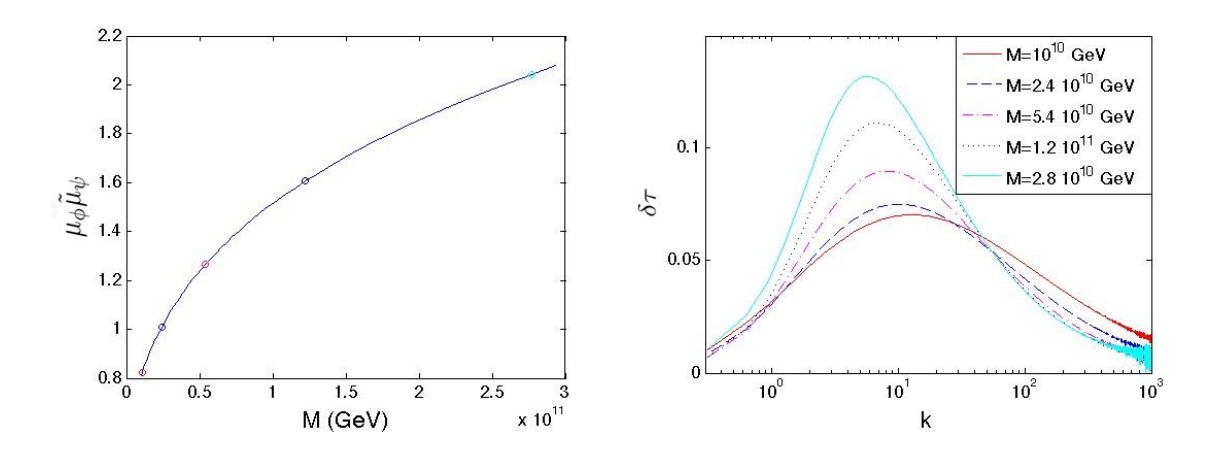

FIG. 13: First Supernatural inflation model with M' at the intermediate scale. Five representative pairs of masses were chosen and the corresponding time delay curves are shown. This model can give maximum time delay of more than 0.1.

ter M are $M = 1.06 \cdot 10^{10}$ GeV, $2.4 \cdot 10^{10}$ GeV, $5.42 \cdot 10^{10}$ GeV, $1.23 \cdot 10^{11}$ GeV, $2.77 \cdot 10^{11}$ GeV. The corresponding pairs of reduced waterfall and timer masses are $\{\mu_\phi, 1/\mu_\psi\} = \{3.19, 4.48\}$, $\{2.58, 2.97\}$, $\{2.22, 2.05\}$, $\{1.99, 1.47\}$, $\{1.83, 1.09\}$. The points on the mass product graph are color coded to match the corresponding time delay curve in Fig. 13. We can see that since the mass products have a larger variation, the resulting spectra have quite different time delay spectra. Also, since the timer is not much lighter than the Hubble scale, the curves do not scale according to our previous analysis.

We finally consider SUSY model 2, Eq. (42), with the $\psi^2\phi^2$ interaction term. Again the
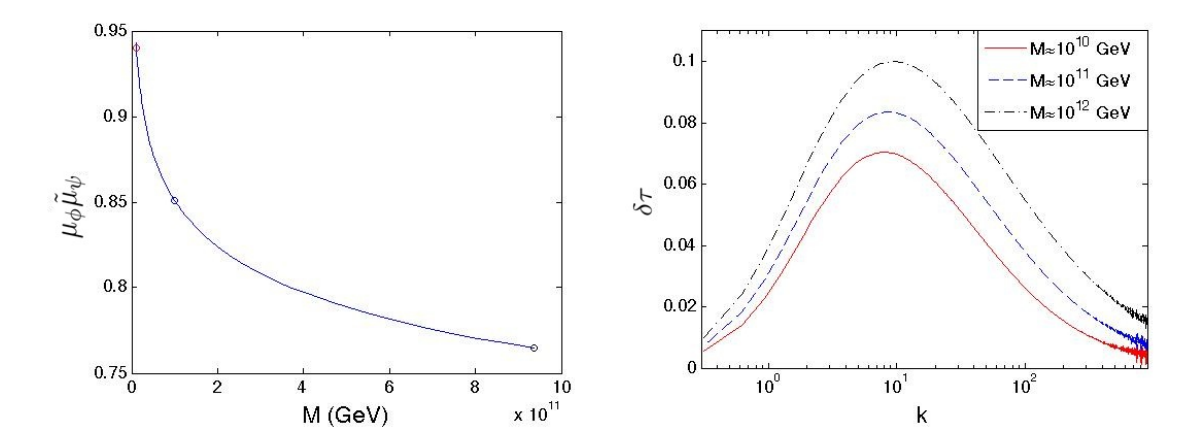
FIG. 14: Second Supernatural inflation model. Three representative pairs of masses were chosen and the corresponding time delay curves are shown.

reduced masses are $O(1)$, so we expect a small λ leading to a large amplitude perturbation spectrum. The mass product varies around 1 by less than $\pm 15\%$. We choose three values of the mass product (the two extrema and an intermediate one) and plot the resulting curves in Fig. 14. The specific values of the mass parameter M are $M = 1.080 \cdot 10^{10}$ GeV, $1.006 \cdot 10^{11}$ GeV, $9.376 \cdot 10^{11}$ GeV and the corresponding pairs of reduced waterfall and timer masses are $\{\mu_\phi, 1/\mu_\psi\} = \{2.697, 2.367\}, \ \{2.330, 2.262\}, \ \{2.007, 2.170\}$.

VII.   CONCLUSIONS

We presented a novel method for calculating the power spectrum of density fluctuations in hybrid inflation, one that does not suffer from the non-existence of a classical field trajectory. We used this method to numerically calculate the power spectrum for a wide range of parameters and concluded that in the case of a light timer field, all characteristics of the power spectrum are controlled by the product of the masses of the two fields. In particular the amplitude was fitted to a power law and found to behave as $\delta\tau_{max} \sim 0.03(\mu_\phi\mu_\psi)^{-0.34}$ and the width in log-space as $\Delta k \sim 1.7(\mu_\phi\mu_\psi)^{-1.17}$. Furthermore we made connection to SUSY inspired models of hybrid inflation and gave numerical results to their power spectra as well. For the SUSY models with a light timer field the numerical results were in excellent agreement with our fitted parameters.

Work is currently under way in refining and extending the formalism. Understanding the rescaling properties between the RSG approximation and the exact result could provide

further insight into the physics of the problem and provide quasi-analytical approximation of well controlled accuracy. We will also apply our results to estimating the number and size of primordial black holes and try to make contact with astrophysical observations regarding supermassive black holes in galactic centers. Finally we are examining the predictions of our model for the non-Gaussian part of the perturbation spectrum.

VIII.   ACKNOWLEDGEMENTS

Appendix A: Zero mode at early times

The $\vec{k} = 0$ mode is not captured by the procedure described in the main text. If we consider this mode alone for asymptotically early times, so that we keep only the exponential in the mass term

$$\ddot{u} + 3\dot{u} = -\mu_\phi^2 e^{-\tilde{\mu}_\psi^2 N} u \tag{A1}$$

This can again be solved in terms of Bessel functions by defining a new variable and a new function as

$$\tilde{z} = \alpha e^{-\tilde{\mu}_\psi^2 N/2} \quad , \quad u(0, N) = \tilde{z}^\beta \tilde{Z}(\tilde{z}) \tag{A2}$$

The mode function becomes

$$\tilde{z}^2 \frac{d^2 \tilde{Z}}{d\tilde{z}^2} + \tilde{z} \frac{d\tilde{Z}}{d\tilde{z}} \left(1 + 2\beta - \frac{6}{\tilde{\mu}_\psi^2} \right) + \tilde{Z} \left(\beta^2 - \frac{6\beta}{\tilde{\mu}_\psi^2} + \frac{\mu_\phi^2 \tilde{z}^2 4}{\alpha^2 \tilde{\mu}_\psi^4} \right) = 0 \tag{A3}$$

The standard form of the differential equation that gives Bessel functions is

$$z^2 \frac{d^2 Z_\nu}{dz^2} + z \frac{dZ_\nu}{dz} + (z^2 - \nu^2) Z_\nu = 0 \tag{A4}$$

By appropriately choosing the constants α, β and ν the two equations can be made identical. The choices are

$$\beta = \frac{3}{\tilde{\mu}_\psi^2} \ , \ \alpha = \frac{2\mu_\phi}{\tilde{\mu}_\psi^2} \ , \ \nu = \frac{3}{\tilde{\mu}_\psi^2} \tag{A5}$$

Finally introducing an arbitrary constant of normalization N_0, the solution for the zero mode at asymptotically early times becomes

$$u(0, N) = N_0 e^{-3N/2} H_\nu^{(1)}(\tilde{z}) \ , \ \tilde{z} = \frac{2\mu_\phi}{\tilde{\mu}_\psi^2} e^{-\tilde{\mu}_\psi^2 N/2} \tag{A6}$$

The normalization factor N_0 can be defined using the Wronskian at early times. The Wronskian at all times is defined as

$$W(\vec{k}, t) = u(\vec{k}, t) \frac{\partial u^*(-\vec{k}, t)}{\partial t} - \frac{\partial u(\vec{k}, t)}{\partial t} u^*(-\vec{k}, t) \tag{A7}$$

Taking the time derivative and using the equation of motion

$$\begin{aligned}
\frac{\partial W(\vec{k}, t)}{\partial t} &= u(\vec{k}, t) \frac{\partial^2 u^*(-\vec{k}, t)}{\partial t^2} - \frac{\partial^2 u(\vec{k}, t)}{\partial t^2} u^*(-\vec{k}, t) = -3HW(\vec{k}, t) \\
&\Rightarrow W(\vec{k}, t) = f(\vec{k}) e^{-3Ht}
\end{aligned} \tag{A8}$$

Since $f(\vec{k})$ is by definition independent of time, we will compute it at approximately early times, where we know the solution in analytic form and the solution is

$$W(\vec{k} \neq 0) = i e^{-3N} \ , \ W(\vec{k} = 0) = \frac{2ir\mu_\psi^2 H}{pi} N_0^2 e^{-3N} \tag{A9}$$

Requiring that the Wronskian be a continuous function of $\vec{k}$ at all times we can extract the value of N_0.

$$N_0 = \sqrt{\frac{3\pi}{2r\mu_\psi^2 H}} \tag{A10}$$

Appendix B: Initial Conditions

We can rewrite the mode equation as a system of three coupled first order differential equations.

$$\frac{d\theta}{dN} = -\frac{\tilde{k} e^{-3N}}{R^2} \tag{B1}$$

$$\frac{dR}{dN} = \dot{R} \tag{B2}$$

$$\frac{d\dot{R}}{dN} = \frac{\tilde{k}^2 e^{-6N}}{R^3} - 3\dot{R} - e^{-2N}\tilde{k}^2 R + \mu_\phi^2(1 - e^{-\tilde{\mu}_\psi^2 N})R \tag{B3}$$

In this notation, $\dot{R}$ is one of the three independent functions.

This is not a system of three coupled ODE's in the strict sense. We can first solve the two equations $\frac{dR}{dN}$ and $\frac{d\dot{R}}{dN}$ as they do not contain any terms involving θ or its derivative. We can then integrate $\frac{d\theta}{dN}$ forward in time, using the calculated values of $R(N)$. Furthermore it is clear that the equations only depend on the magnitude of the wavenumber, as was expected due to the isotropy of the problem, so we need only solve the mode equations for one positive semi axis.

We know from the analytical solution at early times that

$$R(N \to -\infty) \to e^{-N} \tag{B4}$$

Since we have to start the numerical integration at some finite negative time without losing much in terms of accuracy, we refine the initial condition by including extra terms in the above expression. We will then start numerically integrating when our expansion violates the desired accuracy bound. We define the correction to the asymptotic behavior as $\delta R(N)$ such that

$$R(N) \equiv e^{-N} + \delta R(N) \tag{B5}$$

We will expand δR in powers of μ_ϕ^2 and e^N .

$$
\begin{aligned}
\delta R \quad &= \left(\frac{e^N}{2\tilde{k}^2} - \frac{e^{3N}}{8\tilde{k}^4} + \frac{e^{5N}}{16\tilde{k}^6} \right) + \mu_\phi^2 \left(\frac{e^N}{4\tilde{k}^2} \left[1 - e^{-\tilde{\mu}_\psi^2 N} \right] + \frac{e^{3N}}{16\tilde{k}^4} \left[4 + e^{-\tilde{\mu}_\psi^2 N}(\tilde{\mu}_\psi^4 - 6\tilde{\mu}_\psi^2 - 4) \right] \right. \\
&\quad \left. - \mu_\phi^2 \frac{e^{5N}}{64\tilde{k}^6} \left[86 + e^{-\tilde{\mu}_\psi^2 N}(\tilde{\mu}_\psi^8 - 14\tilde{\mu}_\psi^6 + 53\tilde{\mu}_\psi^4 - 25\tilde{\mu}_\psi^2 - 86) \right] \right) \\
&\quad + 5\mu_\phi^4 \left(\frac{e^{3N}}{32\tilde{k}^4} \left[1 - e^{-\tilde{\mu}_\psi^2 N} \right]^2 - \frac{e^{5N}}{64\tilde{k}^6} \left[29 - e^{-\tilde{\mu}_\psi^2 N}(9\tilde{\mu}_\psi^4 - 65\tilde{\mu}\psi^2 + 58) \right. \right. \\
&\quad \left. \left. + e^{-2\tilde{\mu}_\psi^2 N}(14\tilde{\mu}_\psi^4 - 65\tilde{\mu}\psi^2 + 29) \right] \right) + 15\mu_\phi^6 \frac{e^{5N}}{128\tilde{k}^6} \left[1 - e^{-\tilde{\mu}_\psi^2 N} \right]^3 \tag{B6}
\end{aligned}
$$

We can now choose the initial expansion for $R(N)$ to calculate the expansion for the phase $\theta(N)$.

The asymptotic behavior, given by the standard definition of the Hankel functions is

$$\theta(N \to -\infty) = \tilde{k}e^{-N} - \pi \Leftrightarrow \theta(N \to -\infty) + \pi = \tilde{k}e^{-N} \tag{B7}$$

We define $\tilde{\theta} \equiv \theta(N) + \pi \Rightarrow \dot{\tilde{\theta}} = \dot{\theta}$, in order to keep track of the constant phase factor without carrying it through the perturbation expansion.
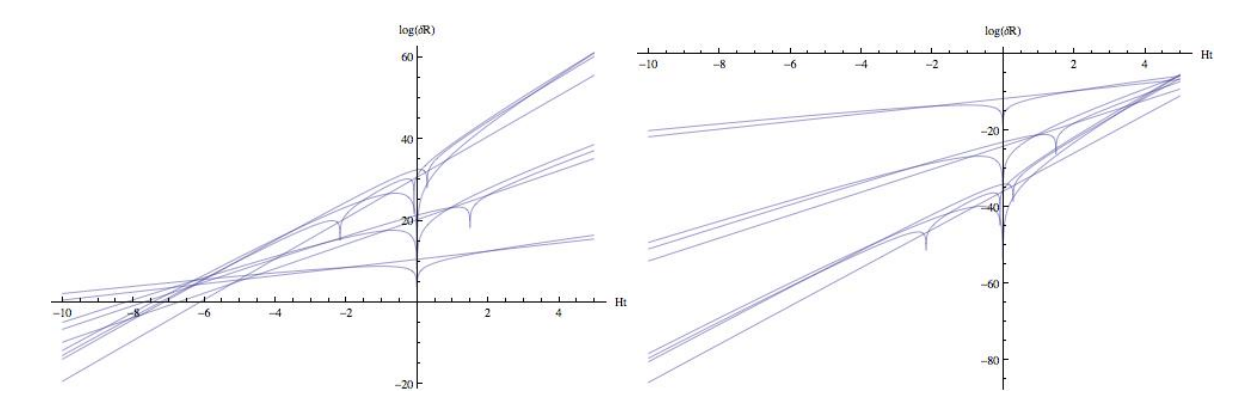
FIG. 15: Mode functions for $\mu_\phi = 22$ and $\tilde{m}u_\psi = 1/18$. The left column is calculated for $\tilde{k} = 1/256$ and the right for $\tilde{k} = 256$

Defining the corrections to the early time behavior of the phase as

$$\tilde{\theta} = e^{-N}[\tilde{k} + \delta\theta(N)] \tag{B8}$$

we can construct a similar expansion as the one for δR. Although our formalism does not require knowledge of $\theta(N)$, we included it for completeness.

---

[1] A. H. Guth, "The inflationary universe: a possible solution to the horizon and flatness problems," Phys. Rev. D **23**, 347 (1981);

A. D. Linde, "A new inflationary universe scenario: a possible solution of the horizon, flatness, homogeneity, isotropy and primordial monopole problems," Phys. Lett. B **108**, 389 (1982);

A. Albrecht and P. J. Steinhardt, "Cosmology for grand unified theories with radiatively induced symmetry breaking," Phys. Rev. Lett. **48**, 1220 (1982).

[2] A. H. Guth and D. I. Kaiser, "Inflationary cosmology: Exploring the universe from the smallest to the largest scales," Science **307**, 884 (2005) [arXiv:astro-ph/0502328].

[3] E. Komatsu et al. [WMAP collaboration], "Seven-year Wilkinson Microwave Anisotropy Probe (WMAP) observations: Cosmological interpretation," Astrophy. J. Suppl. **192**, 18 (2011) [arXiv:1001.4538 [astro-ph.CO]].

[4] F. L. Bezrukov and M. E. Shaposhnikov, "The Standard Model Higgs boson as the inflaton," Phys. Lett. B **659**, 703 (2008) [arXiv:hep-th/0710.3755].

[5] L. Randall, M. Soljacic, and A.H. Guth, "Supernatural Inflation," arXiv:hep-ph/9601296v1.

[6] L. Randall, M. Soljacic, and A.H. Guth, "Supernatural Inflation: Inflation from Supersymmetry with No (Very) Small Parameters," Nucl. Phys. B **472**, 377-408 (1996) [arXiv:hep-ph/9512439v3].

[7] A. Linde, "Hybrid Inflation," Phys. Rev. D **49**, 748-754 (1994) [arXiv:astro-ph/9307002].

[8] J. G. Bellido, A. Linde, and D. Wands, "Density Perturbations and Black Hole Formation in Hybrid Inflation," Phys. Rev. D **54**, 6040-6058 (1996). [arXiv:astro-ph/9605094].

[9] B.J. Carr, "Primordial Black Holes as a Probe of Cosmology and High Energy Physics," Lect. Notes Phys. **631**, 301 (2003) [arXiv: astro-ph/0310838].

[10] B.J. Carr, "Primordial Black Holes–Recent Developments," 22nd Texas Symposium at Stanford, 12-17 December 2004, eConf C **041213**, 0204 (2004) [arXiv:astro-ph/0504034].

[11] B.J. Carr, "Primordial Black Holes: Do They Exist and Are They Useful?" to appear in Proceedings of "Inflating Horizon of Particle Astrophysics and Cosmology," Universal Academy Press Inc and Yamada Science Foundation (2005) [arXiv:astro-ph/0511743].

[12] B.J. Carr, "Primordial black hole formation and hybrid inflation," arXiv:1107.1681 [astro-ph.CO].

[13] K.M. Burgess, "Early Stages in Structure Formation," Ph.D. Thesis, Massachusetts Institute of Technology, 2004.

[14] N.T. Son, "Density Perturbations in Hybrid Inflation," Master's Thesis, Massachusetts Institute of Technology, 2009.

[15] D. Lyth, "Issues concerning the waterfall of hybrid inflation," Prog. Theor. Phys. Suppl. **190**, 107-119 (2011) [arXiv:1005.2461].

[16] D. Lyth, "The hybrid inflation waterfall and the primordial curvature perturbation," [arXiv:astro-ph/1201.4312].

[17] D. Lyth, "Contribution of the hybrid inflation waterfall to the primordial curvature perturbation," JCAP **1107**, 035 (2011) [arXiv:1012.4617].

[18] J. Martin, and V. Vennin, "Stochastic Effects in Hybrid Inflation," Phys. Rev. D **85**, 043525 (2012) [arXiv:1110.2070].

[19] A.A. Abolhasani, H. Firouzjahi, and M. Sasaki, "Curvature perturbation and waterfall dynamics in hybrid inflation," JCAP **1110**, 015 (2011) [arXiv:1106.6315].

[20] H. Kodama, K. Kohri, and K. Nakayama, "On the waterfall behavior in hybrid inflation" [arXiv:1102.5612].

[21] J. Fonseca, M. Sasaki, and D. Wands, "Large-scale Perturbations from the Waterfall Field in Hybrid Inflation," Prog. Theor. Phys. **126**, 331-350 (2011) [arXiv:1005.4053].

[22] A.H. Guth and S.Y. Pi, "Quantum Mechanics of the scalar field in the new inflationary universe," Phys. Rev. D **32**, 1899 (1985).

[23] V. Mukhanov and S. Winitzki, "Introduction to Quantum Effects in Gravity," 2007, Cambridge University Press.

[24] S.W. Hawking, "The development of irregularities in a single bubble inflationary universe," Phys. Lett. B **115**, 295 (1982).

[25] A.H. Guth and S.Y. Pi, "Fluctuations in the new inflationary universe," Phys. Rev. Lett. **49**, 1110 (1982).

[26] A.H. Guth, "Quantum fluctuations in cosmology and how they lead to a multiverse," to be published in the Proceedings of the 25th Solvay Conference in Physics, *The Theory of the Quantum World,* Brussels, October 2011.